The Astrophysical Journal, 782:59 (15pp), 2014 February 20 doi:10.1088/0004-637X/782/2/59

THE CHEMICAL COMPOSITIONS OF RR LYRAE TYPE C VARIABLE STARS

Jose Govea[1], Thomas Gomez[1], George W. Preston[2], and Christopher Sneden[1]

[1] Department of Astronomy and McDonald Observatory, The University of Texas, Austin, TX 78712, USA; jgovea@utexas.edu, chris@verdi.as.utexas.edu

[2] The Observatories of the Carnegie Institution of Washington, Pasadena, CA 91101, USA; iii@ociw.edu

Received 2013 June 5; accepted 2013 November 8; published 2014 January 28

ABSTRACT

We present a detailed chemical abundance study of eight RR Lyrae variable stars of subclass c (RRc). The target RRc stars chosen for study exhibit "Blazhko-effect" period and amplitude modulations to their pulsational cycles. Data for this study were gathered with the echelle spectrograph of the 100 inch du Pont telescope at Las Campanas Observatory. Spectra were obtained throughout each star's pulsation cycle. Atmospheric parameters—effective temperature, surface gravity, microturbulent velocity, and metallicity—were derived at multiple phase points. We found metallicities and element abundance ratios to be constant within observational uncertainties over the pulsational cycles of all stars. Moreover, the α-element and Fe-group abundance ratios with respect to iron are consistent with other horizontal-branch members (RRab, blue and red non-variables). Finally, we have used the [Fe/H] values of these eight RRc stars to anchor the metallicity estimates of a large-sample RRc snapshot spectroscopic study being conducted with the same telescope and instrument combination employed here.

Key words: astrochemistry – stars: abundances – stars: atmospheres – stars: horizontal-branch – stars: variables: general – stars: variables: RR Lyrae

Online-only material: color figures, machine-readable table

1. INTRODUCTION

The H-R diagram positions of low-metallicity stars that are undergoing quiescent helium fusion comprise what we call the horizontal branch (HB). Different metal-poor systems (field stars, globular clusters) exhibit a variety of HBs. Their stars are given labels depending on their surface temperatures (or colors). Members, in order of increasing temperature, are called: red horizontal branch (RHB, 5000 K $\lesssim T_{\rm eff} \lesssim$ 6000 K), RR Lyrae variables (RRab, 6000 K $\lesssim T_{\rm eff} \lesssim$ 7000 K; RRc, 7000 K $\lesssim T_{\rm eff} \lesssim$ 7500 K), blue horizontal branch (BHB, 7500 K $\lesssim T_{\rm eff} \lesssim$ 15,000 K), and, finally, extreme BHB ($T_{\rm eff} \gtrsim$ 15,000 K).

RR Lyrae stars have been studied extensively with photometry and low-resolution spectroscopy, in part because their near-uniform mean brightnesses make them excellent distance indicators. But high-resolution spectroscopic analyses of RR Lyrae are not plentiful, because their short pulsation periods (∼0.1–1.0 days) and large radial-velocity (RV) amplitudes impose limits on exposure times and, consequently, the signal-to-noise ratios (S/Ns) in their spectra. Fortunately, more than 100 RRab stars (see Preston et al. 1991, Appendix) are bright enough to be attractive targets for high-resolution spectroscopy. Nevertheless, studies of atmospheric parameters and abundance analyses are modest in number (Butler et al. 1976, 1979; Clementini et al. 1995; Lambert et al. 1996; For et al. 2011a, 2011b). An extensive study of the eponymous star RR Lyr was conducted by Kolenberg et al. (2010a).

The RRc variables have been neglected in these high-resolution studies; there are fewer RRc's than RRab's and most have been too faint for high-resolution spectroscopy. In this paper, we remedy this situation with the first extensive model atmosphere, metallicity, and abundance ratio study of eight RRc variables observed spectroscopically throughout their pulsational cycles.

The physical origin of the leisurely modulation of light and RV variations in RR Lyrae stars, first recognized by Blazhko (1907), continues to present an intractable puzzle (e.g., Kolenberg et al. 2010b). One long-standing hypothesis, that the effect is produced by the non-uniform surface of an oblique magnetic dipole rotator (Balazs-Detre 1964), has been discredited recently by the failure to detect magnetic fields in excess of ∼100 G in well-studied cases (Chadid et al. 2004; Kolenberg & Bagnulo 2009). Blazhko-like modulations produced by rotational excitation of non-radial pulsation modes are still under scrutiny. However, recent work by Buchler & Kolláth (2011), Gillet (2013), and Cox (2013) has concentrated on exploring interactions between pulsation modes in RR Lyrae stars as a possible explanation for the overall Blazhko effect.

Peterson et al. (1996) reported upper limits to the rotational velocities for 27 field RR Lyrae variables, finding $V \sin i <$ 10 km s^{-1} in all stars. In contrast, multiple investigations (Peterson et al. 1983; Behr 2003a, 2003b) have found many cases of rapid rotation, up to $V \sin i \sim 40$ km s^{-1}, among field and cluster BHB stars. These observations lead to the so-called "Peterson Conundrum" (see Section 3.1 and Figure 4 of Preston 2011): the absence of detectable rotation among RRab stars that should be present when BHBs with high rotational velocities subsequently traverse the RR Lyrae instability strip. G. W. Preston & M. Chadid (in preparation) have devised a method that reduces the upper limit on observed rotation, currently ∼10 km s^{-1}, by a factor of two or more. Thus, the conundrum will become even more of a conundrum. The RRc stars of this paper add to the conundrum database.

Almost all of the objects studied in this paper are a special subset of the RRc variables that Szczygieł & Fabrycky (2007) identified as "Blazhko effect." Szczygieł & Fabrycky (2007) identified these RRc stars to have Blazhko periods of less than 12 days. Their physical properties bear directly on current investigations of not only the Blazhko effect but also the Peterson Conundrum and the variation of microturbulence across the HB. Rotational broadening is noticeable in their spectral lines via $PV = 2\pi R$, in which P, V, and R are the rotation period, axial rotational velocity, and radius of the star. Observed rotation rates less than the predicted values must be

Table 1
Photometric Data for the Program Stars

Star[a] ASAS	Name Variable	V_{min}[b]	V_{max}[b]	$V-K$[c] (mag)	P_{SF07}[d] (days)	$P_{BL,SF07}$[d] (days)	$T_{0,GGPS}$[e] (days)	Class[f] ASAS
081933−2358.2	V701 Pup	10.50	10.70	0.69	0.2856671	−8.10	1869.79	RRC/EC
085254−0300.3		12.40	12.95	0.58	0.2669022	−11.80	1870.30	RRC/EC/ESD
090900−0410.4		10.65	11.10	0.66	0.3032613	−8.11	1869.70	RRC
110522−2641.0		11.70	12.05	0.65	0.2944559	−7.40	1870.50	RRC
162158+0244.5		12.55	13.05	0.72	0.3238044	−8.11	2159.30	RRC
200431−5352.3		10.95	11.30	0.77	0.3002402	+10.82	2174.65	RRC
211933−1507.0	YZ Cap	11.70	12.05	0.65	0.2734570[g]	...	1874.39	...
230659−4354.6	BO Gru	12.70	13.10	0.64	0.2811062	−10.24	1870.45	RRC/EC/ESD

Notes.
[a] In the text, figures, and subsequent tables these star names are abbreviated by the right-ascension portion of their ASAS IDs, e.g., 081933−2358.2 is called AS081933 throughout this paper.
[b] Estimated from the ASAS database.
[c] ASAS database.
[d] A negative value of the Blazhko period means that the additional frequency is smaller than the main pulsation frequency. SF07 = Szczygieł & Fabrycky (2007).
[e] Epoch of light maximum; GGPS = this study.
[f] ASAS suggested stellar classification based on light curve appearance; EC means eclipsing binary, and ESD means eclipsing subdwarf.
[g] This star was not included in the Szczygieł & Fabrycky (2007) study; its pulsational period was determined from our RV data.

attributed to small axial inclinations, and these are amenable to statistical analysis. That test is a work in progress. We only mention that the RRc stars analyzed in this paper belong to the short-period component of the striking bimodal distribution of Blazhko periods identified in Figure 5 of Szczygieł & Fabrycky (2007).

For et al. (2011a) report that microturbulent velocities derived from spectrum analysis vary along the HB, passing through a maximum in the RR Lyrae instability strip. The RRc stars of the present investigation provide new data to assess microturbulence trends in the blue half of the instability strip. Additionally, removal of the microturbulent velocities derived herein by Gaussian deconvolution permits further reduction in the measured limits on rotational velocity.

Kollmeier et al. (2012) have conducted a "snapshot" spectroscopic survey of nearly 250 RRc stars, principally to determine their mean absolute magnitude via statistical parallax. As part of that study, metallicities have been estimated for all of their stars. The present RRc sample gives us the opportunity to anchor the Kollmeier et al. metallicity scale.

In Section 2, we introduce the RRc sample and describe the photometry and spectroscopy of our targets. Atmospheric parameter and abundance determinations are presented in Section 3. We discuss the results in Section 4.

2. OBSERVATIONS, REDUCTIONS, AND RADIAL VELOCITIES

2.1. Target Selection and Photometry

We chose 10 candidate RRc stars for spectroscopic observation. Many of these stars were first identified as RRc variables by the All Sky Automated Survey (ASAS) of Pojmański (2003). This survey monitors the sky photometrically to a limiting magnitude of $V \lesssim 15$ and has resulted in the discovery of large numbers of variable stars. All program stars have ASAS light curves, so throughout the paper we will refer to the stars by the right-ascension part of their ASAS names. For example, star ASAS 081933−2358.2 will be called AS081933. Our target list contains nine stars that were investigated by Szczygieł & Fabrycky (2007) for their Blazhko-effect parameters. We also obtained spectra of the relatively bright RRc star AS211933 (YZ Cap), which is not known to exhibit obvious Blazhko variability.

The target star list included AS144154 (144154−0324.7) and AS204440 (204440−2402.7). However, preliminary examination of our spectra of these stars (Section 2.2) revealed that they have very broad absorption lines. Our RV measurements yielded low mean velocities: −11 km s^{-1} for AS144154 and +16 km s^{-1} for AS204440, which are substantially smaller than we found for the other candidate stars. Finally, these stars have nearly sinusoidal ASAS light curves. These three properties suggest that AS144154 and AS204440 are probably W UMa binaries instead of RR Lyrae stars. They were dropped from further consideration in this study.

The photometric properties of the remaining eight program stars are presented in Table 1; the K magnitudes were obtained from the Two Micron All Sky Survey by Skrutskie et al. 2006). We list approximate minimum and maximum V magnitudes and $V-K$ colors given on the ASAS Web site. Usually $V-K$ colors are excellent indicators of stellar temperatures (e.g., Alonso et al. 1999; Ramírez & Meléndez 2005), but since our stars vary throughout their pulsational cycles by typically $\Delta V \sim 0.4$, the single $V-K$ colors quoted here for each star should be treated merely as representative values.

All but one of the pulsational periods, P_{SF07}, and Blazhko periods, $P_{BL,SF07}$, in Table 1 are taken from Szczygieł & Fabrycky (2007), who describe their methods in detail. They derived pulsational and Blazhko periods in the frequency domain, such that $P = f^{-1}$, where f is the pulsation frequency. The Blazhko period is $P_{BL} = (f_{BL} - f)^{-1}$, so a negative P_{BL} indicates that $f_{BL} < f$. A Blazhko period with a positive sign is attributed by having the additional frequency being larger than the main pulsation frequency. In other words, the Blazhko peak of higher amplitude has a frequency higher than the main pulsation. The lone exception is AS211933, which was not included by Szczygieł & Fabrycky (2007); we quote here the pulsational period derived from our RV data.

2.2. Spectroscopic Observations and Radial Velocities

Our spectra were obtained with the echelle spectrograph of the du Pont 2.5 m telescope at the Las Campanas Observatory.

We observed each program star 6–30 times, mostly covering their complete pulsational phases. Four observing runs during 2009–2010 were partly devoted to this project. The instrumental configuration was identical to that employed for the RRab study of For et al. (2011a, 2011b). The spectrograph was used with the $1.5 \times 4''$ entrance slit, which translates to a resolving power of $R \equiv \lambda/\Delta\lambda \simeq 27{,}000$ at the Mg I b lines near 5180 Å. The total continuous wavelength coverage of the spectra was 3500−9000 Å.

The RRc program stars have photometric pulsational periods of $P \sim 0.3$ days (∼7 hr; Table 1). During their cycles the RVs vary by typically $\Delta RV \sim 20$ km s^{-1} or more. Therefore to avoid excessive RV smearing of the spectral lines, we limited integrations to $t_{obs} \leqslant 20$ minutes, or roughly less than 5% of a pulsational cycle. In fact, only a few exposure times were as long as 20 minutes; most were 15 minutes or less. Therefore broadening of spectral lines due to changing RV was not an issue for our observations. The price paid for time resolution is low photon counts; in a typical extracted spectrum, S/N ∼ 30. In Table 2 we list all of the individual spectra.

We processed the raw spectroscopic data frames with standard IRAF[3] tasks to produce flat-fielded, wavelength-calibrated, multi-order extracted spectra. We derived RVs using the procedure described in Section 4.1 of For et al. (2011a). First, for each observation, we combined 13 echelle orders into a continuous continuum-normalized spectrum. We then used the IRAF *fxcor* task to cross-correlate this spectrum against a template spectrum, fitting a Gaussian to the cross-correlation data to derive the heliocentric RV. The template was created from several spectra of CS 22874009, a blue metal-poor RV standard star (Preston & Sneden 2000) with a T_{eff} similar to those of our RRc stars. This template maximized the cross-correlation signal that minimized RV errors. Table 2 gives the derived RV values for the individual spectra. The minimum and maximum RV values for the stars are summarized in Table 3.

The standard deviation of a single observation made with the du Pont echelle increases with larger apparent magnitude, as indicated by the data in Table 4 of Preston & Sneden (2000). The average standard deviation derived from 69 observations of three stars in that table with $V < 13.5$ (the faint limit of the present study) is 0.67 km s^{-1}. This dispersion—produced by many effects including poor slit illumination due to guiding errors and atmospheric dispersion, spectrograph focus, telescope focus, and instrument flexure—is best estimated by our practice of repeated observations of standard stars. The systematic error of our observations is unknown. We believe that it does not exceed ±1 km s^{-1} based on a comparison of our numerous observations of the metal-poor subgiant HD 140283, whose average RV is −170.92 ± 0.19 km s^{-1} compiled by Kollmeier et al. (2012).

The photometry of ASAS degrades rapidly below $V \sim 12.5$, where our RV data, though sparse, is of superior quality. We employed the now well-established coincidence of light maximum and RV minimum for all RR Lyrae stars to improve the ephemerides of our stars. Adopting the photometric period P_{SF07} as the initial estimate, we altered the P and T_0 until the resulting velocity curves produced maxima at phase $\phi \simeq 0.5$ and minima near $\phi \simeq 0.0$. The resulting estimates of $P_{RV,GGPS}$ and $T_{0,GGPS}$ are entered in Table 3. The velocity variations with these pulsational parameters are shown in the bottom panels of Figures 1−8.

[3] IRAF is distributed by the National Optical Astronomy Observatory, which is operated by the Association of Universities for Research in Astronomy (AURA) under cooperative agreement with the National Science Foundation.

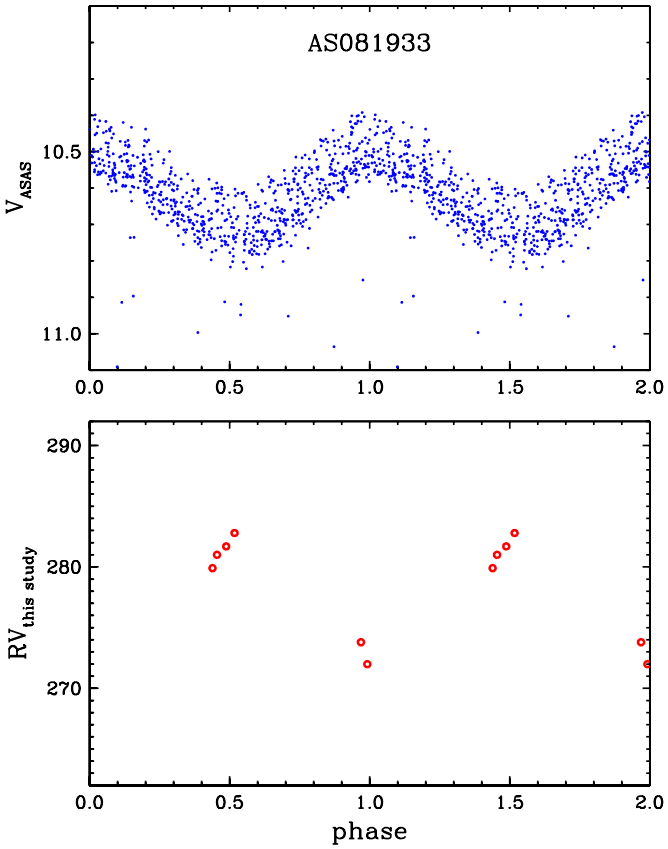

Figure 1. Photometric and RV variations with pulsational phase in the program star AS081933. In the top panel, the ASAS *V* magnitudes are shown, with phases determined from the period P_{SF07} given by Szczygieł & Fabrycky (2007) and *starting epoch*, $T_{0,GGPS}$, determined in this study (Table 1). In the bottom panel, the RV measurements from our spectra are shown, with phases determined in this study (Table 3).

(A color version of this figure is available in the online journal.)

For four of the program stars (AS081933, AS085254, AS090900, and AS200431), either we found P_{SF07} to be adequate or we did not have enough RV data to judge an independent value for the period. As stated earlier, for AS211933 our derived $P_{RV,GGPS}$ was adopted for the photometric data also. For the remaining three stars, we determined $P_{RV,GGPS}$ values that differ slightly from P_{SF07}. Note especially the very noisy photometric light curves for the faint stars AS085254, AS162158, and AS230659. For the latter two stars, $P_{RV,GGPS}$ should be given greater weight than P_{SF07}.

Inspection of the *V* and RV phase curves suggests that the variations in both quantities are well determined and consistent with expectations for RRc stars in the cases of AS110522, AS200431, AS211933, and AS230659 (in this last case, observational data uncertainties limit the information available from the photometry). For AS81933 and AS090900, we did not gather RV data at enough phases to define the velocity curves adequately, but values adopted from P_{SF07} appear to be reasonable. For AS162158, the photometric data are very noisy and it is not easy to discern periodic variations from them. Finally, note that our velocity values for AS085254 vary only by $RV_{min} - RV_{max} = 4.3$ km s^{-1}, whereas the mean of this difference for the other seven stars is 17.6 km s^{-1}. We will comment further on AS085254 in Section 4.

Table 2
Spectroscopic Data

Star	HJD	ϕ	RV (km s^{-1})	$\langle\phi\rangle$	$\langle$RV$\rangle$ (km s^{-1})	Bin Size	S/N[a] (4020–4040 Å)	S/N[a] (5560–5580 Å)
AS081933	5324.4711	0.369	273.76	0.38	280.5	2	61	132
AS081933	5324.4756	0.385	272.01	...	...	...	...	...
AS081933	4904.5545	0.418	279.93	0.43	282.3	2	83	167
AS081933	4904.5630	0.448	281.00	...	...	...	...	...
AS081933	4905.5488	0.899	281.67	0.91	272.9	2	94	167
AS081933	4905.5553	0.922	282.79	...	...	...	...	...
AS085254	4905.5656	0.354	236.42	0.38	236.7	2	29	89
AS085254	4905.5768	0.396	236.92	...	...	...	...	...
AS085254	4904.5734	0.636	239.65	0.66	240.2	2	26	71
AS085254	4904.5832	0.673	240.67	...	...	...	...	...
AS085254	5324.4849	0.915	240.65	0.94	239.2	2	30	77
AS085254	5324.4954	0.954	237.79	...	...	...	...	...

Notes.
[a] S/N ratio presented is obtained from coadded spectrum.
[b] Phases excluded from analysis.

(This table is available in its entirety in a machine-readable form in the online journal. A portion is shown here for guidance regarding its form and content.)

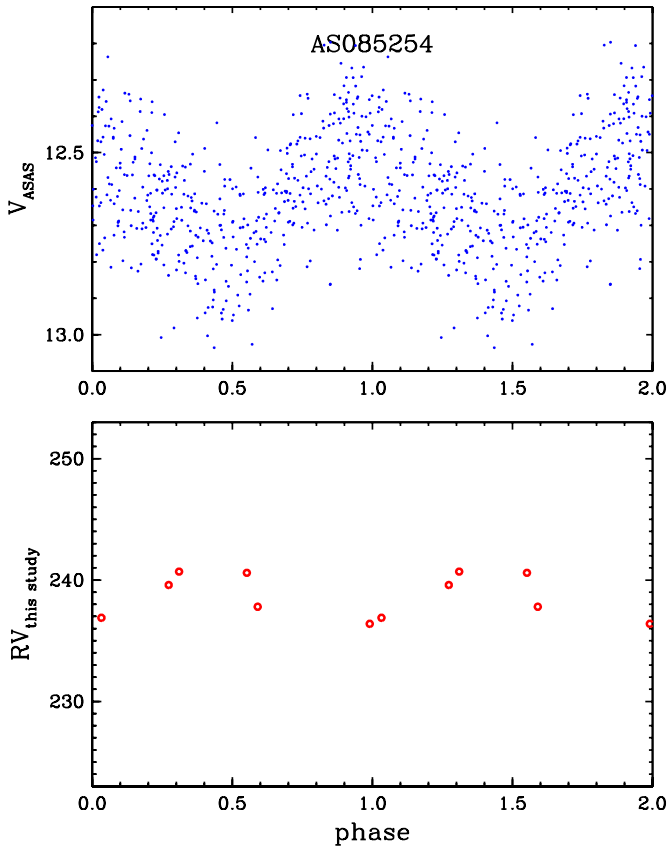

Figure 2. Photometry and RVs for star AS085254, with quantities as described in Figure 1.

(A color version of this figure is available in the online journal.)

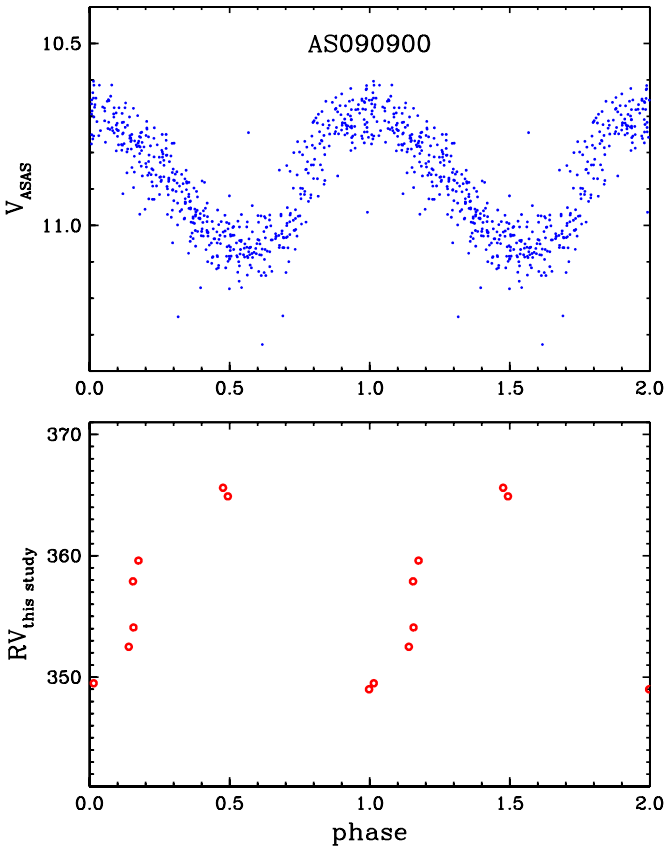

Figure 3. Photometry and RVs for star AS090900, with quantities as described in Figure 1.

(A color version of this figure is available in the online journal.)

3. MODEL ATMOSPHERE AND ABUNDANCE DETERMINATIONS

The 20 minute integration limit yielded spectra that have relatively low S/N values for atmospheric parameter determinations. In order to prepare the spectra for equivalent width (EW) measurements and subsequent chemical composition analysis, we combined the spectra in narrow phase intervals to increase mean S/N ratios. A similar spectrum co-addition technique was employed by For et al. (2011b) in their study of RRab stars using the same telescope, spectrograph, and observational techniques. The co-addition was done by use of the IRAF task *scombine*. The goal was to create as many phase bins as possible throughout a star's pulsation cycle without losing stellar atmospheric information. Individual observations were grouped into phase bins no larger than $\Delta\phi \simeq 0.05$ to minimize contamination due

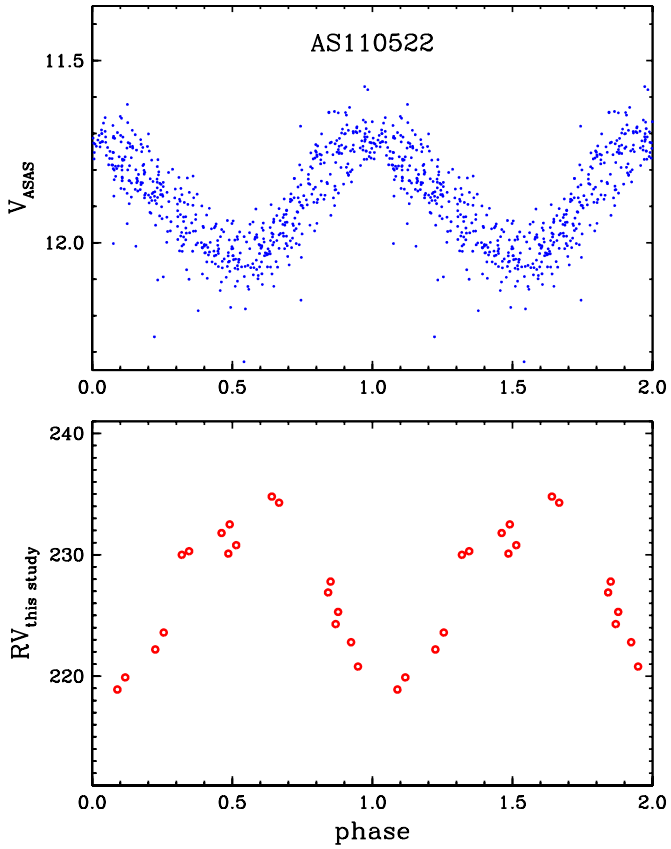

Figure 4. Photometry and RVs for star AS110522, with quantities as described in Figure 1.

(A color version of this figure is available in the online journal.)

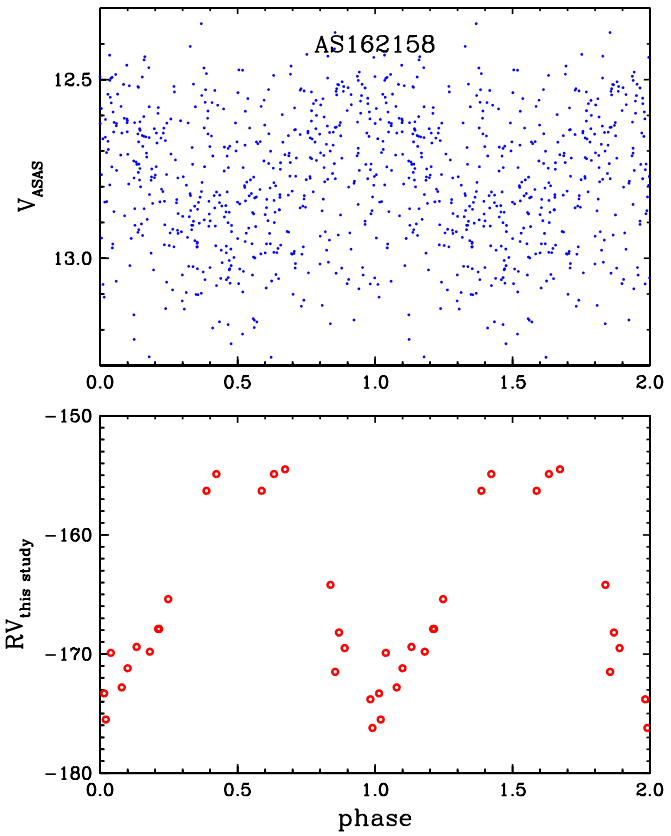

Figure 5. Photometry and RVs for star AS162158, with quantities as described in Figure 1.

(A color version of this figure is available in the online journal.)

Table 3
Radial Velocity Extrema and Pulsation Parameters

Star	RV_{min} (km s^{-1})	RV_{max} (km s^{-1})	$P_{RV,GGPS}$ (days)	$T_{0,GGPS}$ (days)
AS081933	272.0	282.8	0.2856671	4900.180
AS085254	236.4	240.7	0.2669022	4900.400
AS090900	349.0	364.9	0.3032613	4900.200
AS110522	218.9	234.8	0.294510	4900.150
AS162158	−176.2	−154.5	0.323698	4900.435
AS200431	−140.2	−124.5	0.3002402	4900.470
AS211933	−125.7	−100.0	0.2734570	5450.135
AS230659	60.0	77.5	0.2811300	5014.925

to the rapid atmospheric changes. After the co-addition was implemented, we used the IRAF task called *lineclean* to smooth the spectra. In Figure 9, we show a typical example of the co-addition process by plotting the individual spectra and their mean.

Once the spectra were combined, we used the IRAF *lineclean* task to eliminate remaining single-pixel flux anomalies and the *continuum* task to normalize each spectral order. Then for each star in each phase bin, we measured the EWs of all absorption lines that could be reliably detected in the line list of For et al. (2011b). Because our RRc stars are metal poor and 500–1000 K warmer than the RRab stars of For et al., the atomic lines available for analysis in these spectra are weaker and fewer in number. We made EW measurements using our interactive analysis software SPECTRA. This is a semi-automated IDL[4] code that extracts wavelength intensities from the normalized spectra and applies Gaussian line profile fitting to the absorption lines.

As each line was measured, it was visually inspected to make sure that its absorption profile was unblended and not otherwise distorted. Precautions were taken when measuring weak lines that had EW < 20 mÅ. It consistently proved difficult to differentiate between a line and noise regardless of wavelength; this led to large EW uncertainties. For this reason, only a few weak lines were used for the subsequent analysis. Direct integration was done for Sr II and O I lines for which closer inspection was needed.

We derived model atmosphere parameters—$T_{\rm eff}$, log g, v_t, [Fe/H],[5] and relative abundance ratios [X/Fe]—for the program stars at each of their co-added phases. Generally, we followed standard abundance determination methodology, as described in, e.g., For et al. (2011b). We used the current version of the LTE line analysis code MOOG (Sneden 1973)[6] for all calculations. Trial model atmospheres were interpolated from the ATLAS grid (Kurucz 1992)[7] which were calculated assuming α-element enhancements and opacity distribution functions (Castelli &

[4] The Interactive Data Language (IDL) is proprietary software system distributed by Exelis Visual Information Solutions, Inc. Available at http://www.exelisvis.com/ProductsServices/IDL.aspx.

[5] We adopt the standard spectroscopic notation (Helfer et al. 1959) that for elements A and B, $[A/B] \equiv \log_{10}(N_A/N_B)_\star - \log_{10}(N_A/N_B)_\odot$. We use the definition $\log \epsilon(A) \equiv \log_{10}(N_A/N_H) + 12.0$, and equate metallicity with the stellar [Fe/H] value.

[6] Available at http://www.as.utexas.edu/~chris/moog.html.

[7] Available at http://kurucz.harvard.edu/grids.html.

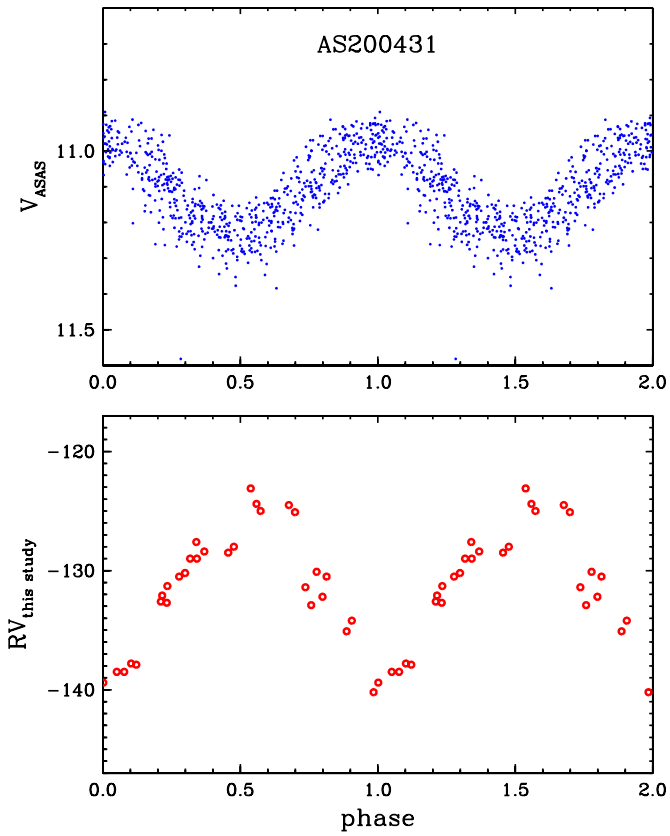

Figure 6. Photometry and RVs for star AS200431, with quantities as described in Figure 1.

(A color version of this figure is available in the online journal.)

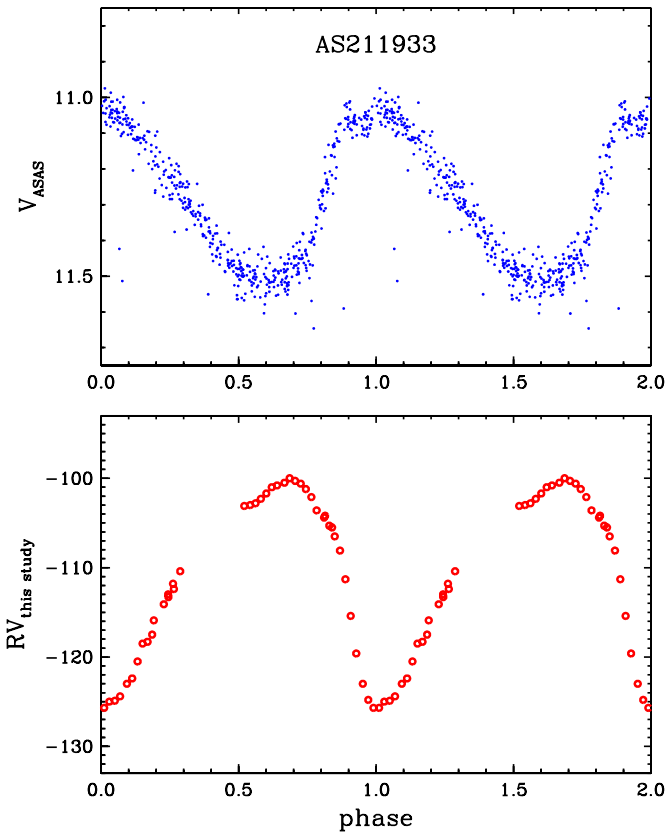

Figure 7. Photometry and RVs for star AS211933 as in Figure 1, except that the pulsational period has been calculated with the RV data of this study.

(A color version of this figure is available in the online journal.)

Kurucz 2003). Interpolation software for the models was kindly given to us by Andy McWilliam and Inese Ivans. The trial model atmospheres and EW line lists were input parameters to the line analysis code MOOG, whose output was individual line abundances from iterative force-fitting of predicted EWs to the measured values.

In performing these computations, we recognized that the ATLAS models were computed for static stellar atmospheres. Clearly that assumption is violated here, as the RRc stars are pulsating on short timescales. Nevertheless, most RR Lyrae abundance studies have been done with similar physical limitations, and For et al. (2011b) have shown that near-constant metallicities and abundance ratios can be determined over the entire pulsation cycles of RRab stars while magnitudes and derived values $T_{\rm eff}$, log g, and v_t are undergoing large variations over their pulsational cycles. We knew before any detailed analyses that the variability in RRc atmospheres must be less severe because the mean max/min change in V for our RRc stars is only $\simeq$0.40 mag (Table 1). Additionally, the light curves for our stars are relatively smooth (Figures 1−8), displaying none of the complexities of RRab light curves that signal the occurrence of the shock-wave phenomena that occur in those stars.

We then altered the input model parameters and repeated the abundance calculations until a model atmosphere was produced, as defined by:

1. $T_{\rm eff}$: no significant trend of abundances with excitation energies of the Fe I lines.
2. log g: agreement within observational/analytical errors of abundances derived from Fe I and Fe II lines.
3. v_t: no significant trend of abundances with reduced EW's of the Fe I lines.
4. Metallicity [M/H]: agreement between assumed model metallicity and derived abundances of Fe.

In Figure 10, we show a typical example of a star's Fe line-by-line abundances after satisfaction of these criteria. The scatter of the points is relatively large, due to the combination of only moderate S/N in the combined spectra and weakness of many of the Fe lines; however the mean abundances are well determined and there are no significant trends with excitation energy, χ, or reduced width, log RW.

4. RESULTS AND DISCUSSION

4.1. Model Atmosphere Parameters

The derived model atmospheric parameters for the program stars at each co-added phase are listed in Table 4. The values of $T_{\rm eff}$, log g, and v_t vary in regular ways throughout the pulsational cycles of each star, and especially the $T_{\rm eff}$ variations mimic those seen in RRab stars (e.g., Figures 13 and 14 of For et al. 2011b). We demonstrate this in Figure 11 by plotting $T_{\rm eff}$ versus phase for all program stars. In the top panel, all the $T_{\rm eff}$'s from Table 4 are shown; on average, the temperatures appear to be lowest near phase $\phi \sim 0.5$ and highest near $\phi \sim 0.0$. However, each star occupies a slightly different place in the RRc domain of the H-R diagram, and its mean $T_{\rm eff}$ will naturally be different from other RRc stars. To show the cyclical temperature changes more clearly, in the lower panel of Figure 11 we have shifted $T_{\rm eff}$ of

Table 4
Model Atmosphere Parameters and Fe Abundances

Star	ϕ	$T_{\rm eff}$ (K)	log g	v_t (km s^{-1})	[M/H]	[Fe/H] Fe I	No. of Lines	σ	[Fe/H] Fe II	No. of Lines	σ
AS081933	0.377	7200	2.50	2.50	−2.50	−2.81	15	0.28	−2.81	7	0.32
AS081933	0.433	7100	2.60	1.70	−2.50	−2.78	14	0.09	−2.84	6	0.10
AS081933	0.911	7400	2.40	2.00	−2.50	−3.07	4	0.14	−3.08	4	0.09
AS085254	0.375	7400	2.40	2.10	−1.50	−1.54	58	0.19	−1.51	35	0.19
AS085254	0.655	7300	2.40	2.40	−1.50	−1.53	59	0.26	−1.55	36	0.26
AS085254	0.935	7500	2.40	2.50	−1.50	−1.52	46	0.31	−1.52	25	0.31
AS090900	0.436	7300	2.00	2.10	−2.00	−1.84	31	0.25	−1.78	22	0.33
AS090900	0.585	7100	2.10	2.00	−2.00	−1.79	43	0.33	−1.80	27	0.34
AS090900	0.914	7100	2.20	2.40	−2.00	−1.75	32	0.31	−1.78	17	0.29
AS110522	0.240	7300	2.10	2.00	−2.00	−1.80	29	0.15	−1.82	19	0.25
AS110522	0.333	7150	2.60	2.00	−2.00	−1.64	40	0.17	−1.65	24	0.39
AS110522	0.488	7100	2.70	1.90	−2.00	−1.79	29	0.22	−1.73	15	0.32
AS110522	0.654	7150	2.50	2.10	−2.00	−1.83	36	0.26	−1.81	23	0.24
AS110522	0.860	7400	2.50	1.80	−2.00	−1.83	28	0.17	−1.77	19	0.28
AS110522	0.937	7500	2.60	2.30	−2.00	−1.82	17	0.17	−1.76	18	0.20
AS162158	0.039	7400	2.10	2.40	−2.00	−1.96	14	0.09	−1.91	18	0.17
AS162158	0.138	7300	2.10	2.00	−2.00	−1.89	11	0.19	−1.82	14	0.25
AS162158	0.225	7100	2.10	2.00	−2.00	−1.83	13	0.18	−1.83	14	0.32
AS162158	0.405	7100	2.10	2.00	−2.00	−1.77	27	0.25	−1.76	15	0.28
AS162158	0.631	7100	2.70	2.40	−2.00	−1.77	44	0.25	−1.83	22	0.16
AS162158	0.863	7400	2.40	2.40	−2.00	−1.79	17	0.21	−1.85	17	0.19
AS200431	0.065	7300	2.30	2.00	−3.00	−2.67	6	0.10	−2.70	5	0.15
AS200431	0.113	7300	2.30	2.00	−3.00	−2.75	5	0.20	−2.76	4	0.13
AS200431	0.224	7200	2.30	1.90	−3.00	−2.67	9	0.16	−2.77	6	0.20
AS200431	0.298	7050	2.00	1.80	−3.00	−2.63	11	0.10	−2.64	7	0.19
AS200431	0.342	6950	2.10	1.70	−3.00	−2.73	12	0.15	−2.77	7	0.08
AS200431	0.467	6950	2.10	1.70	−3.00	−2.67	8	0.13	−2.71	5	0.15
AS200431	0.688	7000	2.10	1.50	−3.00	−2.75	9	0.16	−2.76	7	0.38
AS200431	0.757	7050	2.00	1.50	−3.00	−2.74	12	0.23	−2.74	6	0.09
AS200431	0.994	7300	2.30	1.70	−3.00	−2.78	4	0.31	−2.76	6	0.31
AS211933	0.250	7000	2.20	2.50	−1.50	−1.48	84	0.21	−1.45	43	0.21
AS211933	0.550	6800	2.30	2.50	−1.50	−1.53	97	0.18	−1.50	42	0.22
AS211933	0.630	6800	2.30	2.30	−1.50	−1.53	94	0.27	−1.49	38	0.23
AS211933	0.720	7000	2.40	2.50	−1.50	−1.49	83	0.16	−1.44	35	0.19
AS211933	0.808	7300	2.20	2.70	−1.50	−1.54	44	0.14	−1.48	28	0.25
AS211933	0.890	7400	2.20	2.70	−1.50	−1.53	43	0.17	−1.45	31	0.24
AS211933	0.991	7400	2.10	2.70	−1.50	−1.52	40	0.13	−1.49	27	0.25
AS230659	0.096	7300	2.10	2.10	−2.00	−1.78	35	0.21	−1.80	22	0.21
AS230659	0.247	7000	2.00	2.00	−2.00	−1.78	31	0.33	−1.80	22	0.34
AS230659	0.340	7100	1.90	2.00	−2.00	−1.88	39	0.12	−1.88	24	0.25
AS230659	0.385	7050	1.90	2.00	−2.00	−1.85	30	0.29	−1.85	27	0.35
AS230659	0.543	6950	1.80	2.30	−2.00	−1.83	43	0.28	−1.82	27	0.36
AS230659	0.679	7000	2.10	2.30	−2.00	−1.78	47	0.31	−1.85	24	0.25
AS230659	0.711	7100	2.20	2.40	−2.00	−1.81	41	0.24	−1.86	27	0.21
AS230659	0.856	7100	2.20	2.20	−2.00	−1.79	41	0.29	−1.83	21	0.28
AS230659	0.904	7200	2.10	2.20	−2.00	−1.80	36	0.23	−1.84	23	0.28
AS230659	0.976	7250	2.10	2.20	−2.00	−1.85	28	0.23	−1.82	21	0.24

four of our program stars (AS200431, AS211933, AS085254, and AS230659) by +160 K, +150 K, −200 K, and +125 K, respectively, to roughly match the $T_{\rm eff}$ of AS110522 near $\phi \approx$ 0.30–0.45. The regularity of the temperature variations is much more apparent and shows that all the RRc stars in our sample pulsate in similar fashions.

The atmospheric parameter variations for our RRc sample should be smaller than those of the RRab stars because the brightness and radius variations of the RRc's are small compared to those for the RRab's. For the 11 RRab stars studied by For et al. (2011a, 2011b), the mean max/min excursions in atmospheric parameters are ≃1250 K in $T_{\rm eff}$, ≃1.0 dex in log g, and ≃1.3 km s^{-1} in v_t. From the data of Table 4, mean min/max values for our RRc sample are ≃350 K in $T_{\rm eff}$, ≃0.3 dex in log g, and ≃0.6 km s^{-1} in v_t. These variations are roughly a third for the RRab stars.

The RRc target AS085254 deserves special mention here. In Section 2.2, we called attention to the relatively small RV changes in this star over its pulsational cycles that were covered by our spectroscopic observations. We note that AS085254 has a similarly small effective temperature range, 7300−7500 K, and at no phase does $T_{\rm eff}$ get as low as 7100 K, in contrast to all other program stars. Additionally, the $V-K$ color of AS085254 is much less than other stars. We suggest that this star is probably near the blue edge of the RR Lyrae instability strip and only mildly unstable at the present epoch.

In Figure 12, we show the variation in microturbulent velocities with effective temperatures for several HB groups. The rise

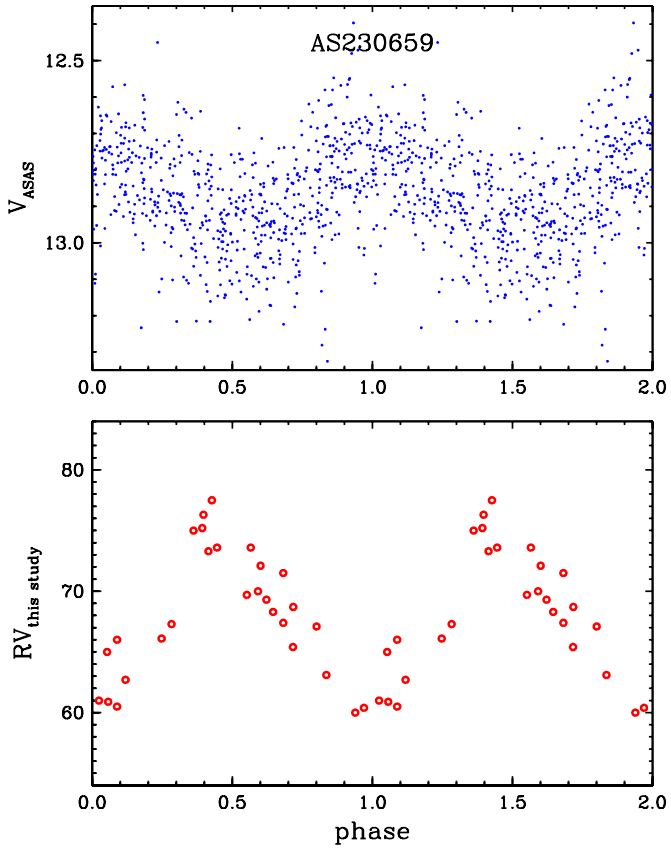

Figure 8. Photometry and RVs for star AS230659, with quantities as described in Figure 1.

(A color version of this figure is available in the online journal.)

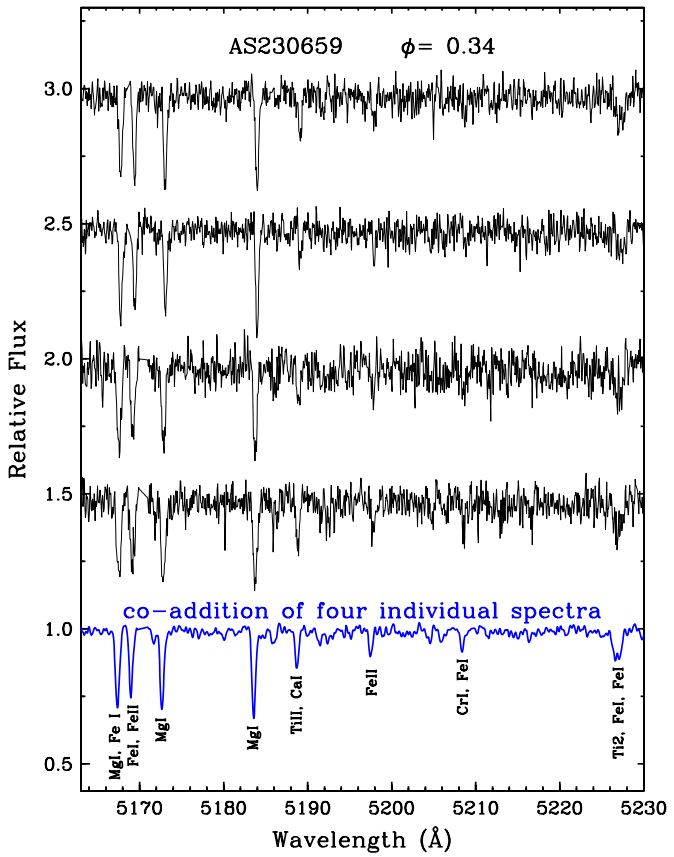

Figure 9. Example of spectrum co-addition after applying IRAF task *lineclean* to smooth the spectra. Four individual spectra (shown in black) with exposure times 8−10 minutes each were obtained for AS230659 near pulsational phase $\phi = 0.34$. The wavelength range near the Mg I b lines is displayed because it contains many strong lines, several of which are labeled at the bottom of the figure. Many other spectral domains are nearly line free in this warm, very metal-poor RRc star. The co-addition of these four spectra (shown in blue) is an example of the kinds of spectra analyzed for atmospheric parameters and abundances in this study. The vertical scale for the co-added spectrum is correct, and vertical shifts have been applied to the other spectra for display purposes.

(A color version of this figure is available in the online journal.)

in v_t with increasing $T_{\rm eff}$ among RHB stars has been documented previously (Preston et al. 2006; For & Sneden 2010). Derived microturbulence values appear to peak for both the warmest RHB stars and the RRab stars at $v_t \lesssim 3.5$ km s^{-1} and decline to ∼2 km s^{-1} for BHB stars, albeit with significant star-to-star scatter. Our RRc sample adds additional information on the warmer HB stars. It is clear from Figure 12 that the v_t among RRc variables at ϕ's ≈ 0.35 is sharply lower than the mean v_t among the RRab's. For & Sneden (2010) derived some larger v_t values in a few of their BHB stars, but all of these cases turned out to be rapid rotators. By adopting the $v \sin i$ values determined by Behr (2003b), we have separated BHB stars with $v \sin i < 15$ km s^{-1} and BHB stars with $v \sin i > 15$ km s^{-1} in Figure 12. All but one of the slow rotators have $v_t < 2.5$ km s^{-1}, in accordance with the RRc microturbulence values. The larger v_t values of a few BHB stars may be a real stellar atmosphere effect or may signal the intrinsic difficulty in extracting accurate microturbulent velocities of rapidly rotating stars; that issue is beyond the scope of our work. What is clear here is that large v_t values are mostly a property of warmer RHB and RRab stars.

4.2. Abundances

We list the [X/Fe] values for each star at each co-added phase in Tables 5 and 6, and mean values for each star in Table 7. Figures 13 and 14 show the RRc abundance ratios along with those of RHB and BHB stars (For & Sneden 2010) and those of RRab stars (For et al. 2011b) as functions of [Fe/H] metallicity. Figures 15 and 16 show the same abundances as functions of $T_{\rm eff}$. The "internal" atmospheric parameter uncertainties, which are defined here as the uncertainties in determining these parameters from the criteria described in Section 3, are estimated to be ±300 K in $T_{\rm eff}$ and ±0.3 in log g, v_t, and [M/H]. We have simulated the effects of the resulting uncertainties in the abundances by varying the input parameters by these amounts; the changes are small. Taking Fe as the reference metallicity, for $\Delta T_{\rm eff} = \pm 150$ K, Δ[Fe I] = ±0.13 and Δ[Fe II] = ±0.06. The derived metallicity rises with increasing $T_{\rm eff}$ due to the increase in continuum opacity—more for Fe I because it is almost completely ionized. For $\Delta \log g = \pm 0.3$, Δ[Fe I] = ±−0.01 and Δ[Fe II] = ±0.10; gravity changes affect the majority of Fe II species but not so for Fe I. For $\Delta v_t = \pm 0.3$, Δ[Fe I] = ±−0.04 and Δ[Fe II] = ±−0.05; lines of comparable strength are affected equally by microturbulence changes, regardless of ionization state. Finally, Δ[M/H] = ±0.3 produces essentially no abundance changes; the atmospheric structures of warm ($T_{\rm eff} > 7000$ K), metal-poor ([M/H] < −1.5) stars are mostly insensitive to metal-line blanketing.

Additionally, the responses to the abundances of the neutral species to atmospheric parameter changes closely mimic those of Fe I and the ionic species react similarly to Fe II, so the relative abundance ratios do not critically depend on parameter

Table 5
Abundance Ratios [X/Fe] for Elements Na through Ti

Star	ϕ[a]	Na[b]	#[c]	σ[d]	Mg	#	σ	Al	#	σ	Si I	#	σ	Si II	#	σ	Ca I	#	σ	Sc II	#	σ	Ti II	#	σ
AS081933	0.377	0.02	2	0.32	0.40	2	0.15	−0.39	2	0.07	0.11	1	0.00	1.53	1	0.00	0.43	1	0.00	0.31	2.00	0.24	0.42	16	0.17
AS081933	0.433	0.09	2	0.42	−0.07	4	0.29	−0.58	2	0.07	0.13	1	0.00	...	...	...	0.38	1	0.00	0.14	2.00	0.08	0.36	16	0.10
AS081933	0.911	0.28	2	0.23	0.55	3	0.21	...	...	...	0.52	1	0.00	0.80	1	0.00	0.29	1	0.00	0.33	1.00	0.00	0.52	10	0.10
AS085254	0.375	0.08	2	0.29	0.33	5	0.32	−0.71	2	0.07	0.26	1	0.00	0.00	4	0.29	0.18	8	0.30	0.02	5.00	0.15	0.34	29	0.24
AS085254	0.655	0.40	2	0.03	0.54	4	0.26	−0.67	2	0.04	−0.04	1	0.00	0.06	5	0.12	0.25	9	0.13	0.02	4.00	0.04	0.24	30	0.23
AS085254	0.935	0.25	2	0.01	0.38	6	0.58	−0.71	2	0.26	1.31	2	1.31	0.06	3	0.28	0.30	3	0.30	0.16	4.00	0.15	0.21	25	0.30
AS090900	0.436	0.35	2	0.09	0.62	3	0.22	−0.58	2	0.34	−0.19	1	0.00	0.30	4	0.64	0.45	3	0.09	0.21	2.00	0.03	0.23	26	0.23
AS090900	0.585	0.46	2	0.15	0.66	4	0.31	−0.31	1	0.00	0.00	1	0.00	0.61	4	0.72	0.36	5	0.16	0.12	3.00	0.21	0.34	27	0.26
AS090900	0.914	0.51	2	0.12	0.59	4	0.21	−0.53	2	0.06	−0.78	1	0.00	−0.42	1	0.00	0.51	7	0.27	0.13	3.00	0.16	0.16	23	0.22
AS110522	0.240	0.15	2	0.15	0.45	3	0.44	−0.34	2	0.05	...	...	...	...	...	...	0.45	3	0.00	0.30	3.00	0.01	0.25	23	0.22
AS110522	0.333	−0.02	2	0.13	0.30	3	0.65	−0.73	2	0.17	−0.33	1	0.00	0.19	2	0.18	0.39	3	0.42	0.30	2.00	0.09	0.39	21	0.28
AS110522	0.488	−0.25	2	0.09	0.48	3	0.23	...	...	...	...	...	...	0.59	1	0.00	0.21	6	0.15	0.05	2.00	0.00	0.26	20	0.37
AS110522	0.654	−0.03	2	0.28	0.47	5	0.23	−0.83	1	0.00	...	...	...	...	...	...	0.57	5	0.17	0.12	3.00	0.20	0.34	25	0.18
AS110522	0.860	−0.02	2	0.02	0.31	4	0.48	−0.94	1	0.00	−0.18	1	0.00	0.53	1	0.00	0.28	3	0.00	0.09	3.00	0.06	0.39	19	0.21
AS110522	0.937	−0.05	2	0.16	0.38	4	0.25	−0.52	1	0.00	−0.34	1	0.00	0.23	2	0.34	0.70	1	0.00	0.16	2.00	0.04	0.34	20	0.17
AS162158	0.039	0.40	1	0.00	0.58	4	0.06	−0.08	1	0.00	−0.01	1	0.00	0.60	2	0.04	0.22	2	0.10	0.03	2.00	0.08	0.22	17	0.19
AS162158	0.138	0.46	2	0.23	0.45	4	0.13	−0.01	1	0.00	...	...	...	0.58	2	0.08	0.07	1	0.00	0.09	2.00	0.08	0.32	18	0.25
AS162158	0.225	0.19	2	0.14	0.56	4	0.05	−0.50	1	0.07	...	...	...	0.62	2	0.26	0.06	1	0.03	0.20	2.00	0.13	0.29	20	0.25
AS162158	0.405	0.78	2	0.31	0.25	3	0.40	...	...	...	...	...	...	0.51	1	0.00	0.22	5	0.46	0.11	2.00	0.73	0.09	17	0.42
AS162158	0.631	0.31	2	0.63	0.36	5	0.15	−0.83	2	0.00	0.23	1	0.00	0.35	2	0.07	0.44	5	0.50	−0.09	3.00	0.54	0.30	22	0.20
AS162158	0.863	0.40	2	0.43	0.48	4	0.28	−0.59	2	0.00	−0.21	1	0.00	0.44	3	0.81	0.06	2	0.00	0.06	2.00	0.11	0.23	20	0.24
AS200431	0.065	...	...	...	0.54	2	0.01	...	...	...	0.10	1	0.00	...	...	...	0.09	1	0.00	−0.08	1.00	0.00	0.36	11	0.18
AS200431	0.113	...	...	...	0.52	2	0.02	...	...	...	...	...	...	...	...	...	0.05	1	0.00	...	...	...	0.34	10	0.18
AS200431	0.224	−0.15	2	0.20	0.55	2	0.18	...	...	...	...	...	...	...	...	...	0.33	1	0.00	0.09	1.00	0.00	0.34	11	0.20
AS200431	0.298	−0.01	2	0.03	0.52	2	0.21	−0.35	1	0.00	0.13	1	0.00	...	...	...	0.09	1	0.00	−0.02	1.00	0.00	0.34	14	0.19
AS200431	0.342	0.12	2	0.15	0.43	2	0.16	−0.48	1	0.00	...	...	...	...	...	...	0.41	1	0.00	−0.01	1.00	0.00	0.33	15	0.19
AS200431	0.467	−0.09	2	0.01	0.40	2	0.35	...	...	...	...	...	...	...	...	...	0.10	2	0.03	−0.13	1.00	0.00	0.25	13	0.16
AS200431	0.688	−0.31	1	0.00	0.62	2	0.00	−0.55	1	0.00	...	...	...	1.22	1	0.00	0.23	1	0.00	0.22	3.00	0.43	0.60	12	0.50
AS200431	0.757	−0.04	1	0.00	0.45	3	0.14	−0.55	2	0.00	−0.07	1	0.00	...	...	...	0.02	1	0.00	−0.33	1.00	0.00	0.26	13	0.14
AS200431	0.994	0.41	1	0.00	0.45	2	0.28	...	...	...	...	...	...	...	...	...	0.04	1	0.00	...	...	...	0.28	10	0.12
AS211933	0.250	0.52	2	0.16	0.58	4	0.13	−0.60	2	0.02	0.51	1	0.00	0.51	4	0.08	0.29	12	0.10	−0.05	6.00	0.16	0.25	33	0.19
AS211933	0.550	0.60	2	0.21	0.57	2	0.24	−0.82	2	0.37	−0.04	1	0.00	0.46	5	0.16	0.31	14	0.14	0.11	5.00	0.24	0.32	34	0.25
AS211933	0.630	0.51	1	0.00	0.65	4	0.20	−0.95	2	0.02	−0.40	1	0.00	0.45	4	0.18	0.33	14	0.11	−0.04	6.00	0.18	0.30	35	0.22
AS211933	0.720	0.37	1	0.00	0.70	4	0.31	−0.85	2	0.22	−0.18	1	0.00	0.66	5	0.61	0.29	11	0.14	0.05	4.00	0.23	0.36	34	0.23
AS211933	0.808	0.27	2	0.14	0.74	4	0.34	−0.67	2	0.31	...	...	...	0.37	4	0.18	0.28	8	0.09	−0.08	3.00	0.22	0.34	26	0.21
AS211933	0.890	0.34	2	0.17	0.88	4	0.41	−0.53	2	0.24	−0.10	1	0.00	0.50	3	0.27	0.27	8	0.07	−0.04	3.00	0.15	0.44	24	0.27
AS211933	0.991	0.29	2	0.21	0.64	4	0.19	−0.63	2	0.23	−0.16	1	0.00	0.37	4	0.22	0.28	6	0.08	−0.07	4.00	0.08	0.26	25	0.14
AS230659	0.096	0.43	2	0.10	0.82	4	0.31	0.07	1	0.00	...	...	...	0.42	2	0.19	0.65	3	0.08	0.06	3.00	0.27	0.31	25	0.23
AS230659	0.247	0.19	2	0.24	0.15	4	0.76	−0.67	1	0.00	−0.28	1	0.00	0.47	3	0.23	−0.14	3	0.25	−0.37	3.00	0.39	0.19	20	0.24
AS230659	0.340	0.58	2	0.11	0.70	5	0.13	−0.31	2	0.04	−0.49	1	0.00	0.67	4	0.29	0.36	6	0.06	0.15	2.00	0.35	0.33	22	0.28
AS230659	0.385	0.72	2	0.40	0.46	4	0.32	−0.36	2	0.34	−0.33	1	0.00	0.72	4	0.38	0.45	4	0.10	−0.20	3.00	0.47	0.30	24	0.42
AS230659	0.543	0.74	2	0.21	0.64	6	0.23	−0.72	2	0.51	−0.23	1	0.00	0.38	4	0.30	0.16	8	0.23	−0.19	4.00	0.20	0.22	23	0.24
AS230659	0.679	0.70	3	0.15	0.60	4	0.32	−0.54	2	0.21	0.03	1	0.00	0.66	4	0.13	0.34	9	0.30	−0.12	3.00	0.36	0.15	22	0.25
AS230659	0.711	0.83	2	0.27	0.76	4	0.34	0.05	1	0.00	−0.63	1	0.00	0.55	4	0.13	0.46	9	0.21	−0.04	2.00	0.19	0.37	23	0.36
AS230659	0.856	0.71	2	0.11	0.82	3	0.30	−0.78	2	0.56	−0.33	1	0.00	0.42	4	0.36	0.25	7	0.22	−0.04	4.00	0.18	0.32	25	0.33
AS230659	0.904	0.48	2	0.24	0.83	4	0.24	−0.28	1	0.00	−0.17	1	0.00	0.59	4	0.42	0.26	3	0.13	0.16	2.00	0.09	0.40	28	0.30
AS230659	0.976	0.43	2	0.08	0.48	4	0.42	−0.34	1	0.00	0.36	1	0.00	0.46	5	0.49	0.35	3	0.11	0.30	3.00	0.13	0.33	24	0.24

Notes.
[a] Mean phase of co-added spectrum.
[b] All abundance units are [X/Fe].
[c] Number of lines.
[d] Sample standard deviation.

Table 6
Abundance Ratios [X/Fe] for Elements Cr through Ba

Star	ϕ[a]	Cr I[b]	#[c]	σ[d]	Cr II	#	σ	Ni I	#	σ	Sr II	#	σ	Y II	#	σ	Ba II	#	σ
AS081933	0.377	−0.11	1	0.00	...	...	...	...	...	...	0.27	1	0.29	...	...	...	...	...	...
AS081933	0.433	−0.04	2	0.17	...	...	...	...	...	...	0.30	2	0.34	...	...	...	...	...	...
AS081933	0.911	...	...	...	...	...	...	...	...	...	−0.23	1	0.00	...	...	...	...	...	...
AS085254	0.375	−0.28	5	0.31	0.04	8	0.21	...	...	...	0.56	2	0.19	...	...	...	0.03	1	0.00
AS085254	0.655	−0.11	4	0.12	0.01	4	0.16	...	...	...	0.75	2	0.10	...	...	...	0.22	1	0.00
AS085254	0.935	−0.14	4	0.18	−0.12	4	0.26	...	...	...	0.40	2	0.10	−0.30	1	0.37	0.10	1	0.00
AS090900	0.436	−0.25	3	0.19	−0.07	6	0.15	...	...	...	0.21	2	0.23	...	...	...	0.15	1	0.00
AS090900	0.585	−0.15	4	0.24	0.06	5	0.18	...	...	...	0.59	2	0.01	0.21	2	0.56	0.39	1	0.00
AS090900	0.914	−0.03	3	0.20	−0.07	1	0.00	0.44	1	0.00	0.73	2	0.30	0.05	1	0.00	0.60	1	0.00
AS110522	0.240	−0.16	2	0.00	0.01	3	0.00	...	...	...	0.81	1	0.00	...	...	...	0.05	1	0.00
AS110522	0.333	−0.11	2	0.10	0.07		0.39	...	...	...	0.15	2	0.71	0.19		0.00	0.31	1	0.00
AS110522	0.488	0.02	1	0.00	0.27	3	0.24	...	...	...	0.71	2	0.04	...	...	...	0.02	1	0.00
AS110522	0.654	−0.04	4	0.27	0.20	4	0.26	...	...	...	0.27	2	0.15	...	...	...	0.34	1	0.00
AS110522	0.860	−0.13	2	0.08	0.17	2	0.26	...	...	...	−0.05	2	0.10	...	...	...	0.07	1	0.00
AS110522	0.937	...	...	...	0.23	1	0.00	...	...	...	0.04	2	0.07	...	...	...	...	...	...
AS162158	0.039	0.03	1	0.00	0.11	1	0.09	...	...	...	0.05	2	0.64	...	...	...	...	...	...
AS162158	0.138	0.09	2	0.39	0.03	3	0.08	...	...	...	0.46	2	0.64	...	...	...	...	...	...
AS162158	0.225	−0.31	1	0.00	0.08	3	0.14	...	...	...	−0.02	2	0.35	0.64	2	0.49	−0.15	1	0.00
AS162158	0.405	−0.38	3	0.27	−0.04	3	0.34	...	...	...	0.03	2	1.07	−0.15	1	0.00	...	...	...
AS162158	0.631	−0.29	3	0.28	0.14	2	0.09	...	...	...	0.02	2	0.88	...	...	...	...	...	...
AS162158	0.863	−0.27	2	0.01	0.08	1	0.00	...	...	...	−0.23	2	0.51	...	...	...	...	...	...
AS200431	0.065	...	...	...	...	...	...	...	...	...	−0.45	1	0.00	...	...	...	...	...	...
AS200431	0.118	...	...	...	...	...	...	...	...	...	−0.22	2	0.00	...	...	...	...	...	...
AS200431	0.224	−0.22	1	0.00	0.24	1	0.00	...	...	...	0.03	2	0.42	...	...	...	...	...	...
AS200431	0.298	...	...	...	0.34	1	0.00	...	...	...	0.15	2	0.32	...	...	...	...	...	...
AS200431	0.342	0.13	1	0.00	...	...	...	...	...	...	0.03	2	0.40	...	...	...	...	...	...
AS200431	0.467	−0.41	2	0.11	−0.02	1	0.00	...	...	...	−0.04	2	0.42	...	...	...	...	...	...
AS200431	0.688	0.71	3	0.51	...	...	...	...	...	...	0.02	2	0.33	...	...	...	...	...	...
AS200431	0.757	−0.25	1	0.00	0.34	1	0.00	...	...	...	−0.30	2	0.59	...	...	...	...	...	...
AS200431	0.994	...	...	...	...	...	...	...	...	...	...	...	...	...	...	...	...	...	...
AS211933	0.250	−0.20	6	0.31	0.00	8	0.14	...	...	...	0.57	2	0.65	0.08	3	0.20	...	...	...
AS211933	0.550	−0.10	5	0.16	0.02	6	0.14	0.45	1	0.00	1.02	2	0.26	0.12	3	0.35	...	...	...
AS211933	0.630	−0.15	4	0.23	0.00	7	0.16	...	...	...	0.81	2	0.23	0.11	3	0.12	...	...	...
AS211933	0.720	−0.11	4	0.14	0.07	6	0.11	...	...	...	1.06	2	0.23	0.16	2	0.12	...	...	...
AS211933	0.808	−0.16	3	0.14	0.03	5	0.14	...	...	...	0.46	2	0.14	...	...	...	−0.09	1	0.00
AS211933	0.890	−0.20	4	0.10	0.05	5	0.13	...	...	...	0.50	2	0.31	...	...	...	−0.14	1	0.00
AS211933	0.991	−0.21	3	0.12	0.01	5	0.15	...	...	...	0.17	2	0	...	...	...	−0.16	1	0.00
AS230659	0.096	−0.25	2	0.09	−0.08	5	0.13	...	...	...	1.08	2	0.35	0.25	1	0.00	0.22	1	0.00
AS230659	0.247	−0.60	3	0.15	−0.06	5	0.22	...	...	...	1.45	1	0.00	−0.15	1	0.00	0.14	1	0.00
AS230659	0.340	−0.19	3	0.15	0.28	2	0.03	...	...	...	1.24	2	0.39	0.07	1	0.00	0.34	1	0.00
AS230659	0.385	−0.28	3	0.20	0.14	7	0.29	...	...	...	1.21	2	0.52	0.23	2	0.21	0.18	1	0.00
AS230659	0.543	−0.20	1	0.00	0.13	3	0.21	...	...	...	0.85	2	0.65	0.21	2	0.12	−0.05	1	0.00
AS230659	0.679	−0.12	4	0.17	0.11	4	0.21	...	...	...	0.76	2	0.47	0.72	3	0.20	0.14	1	0.00
AS230659	0.711	−0.03	4	0.21	0.13	5	0.17	...	...	...	0.66	2	0.83	0.82	2	0.18	0.11	1	0.00
AS230659	0.856	−0.08	3	0.15	−0.11	3	0.30	...	...	...	1.42	2	0.16	0.69	2	0.41	0.22	1	0.00
AS230659	0.904	−0.09	4	0.09	0.21	3	0.24	...	...	...	0.46	2	0.52	0.33	1	0.00	0.21	1	0.00
AS230659	0.976	−0.06	3	0.13	0.12	4	0.09	...	...	...	1.07	2	0.10	...	...	...	0.19	1	0.00

Notes.
[a] Mean phase of co-added spectrum.
[b] All abundance units are [X/Fe].
[c] Number of lines.
[d] Sample standard deviation.

uncertainties. The reader of course should be alert to these arguments applying strictly to our LTE, static model approximations. Further exploration of the adequacies of these analytical limitations will be welcome.

The mean metallicity of our RRc program stars is [Fe/H] $\simeq -2.0$ and the median is [Fe/H] $\simeq -1.8$, a value intermediate between those of the inner and outer halo populations identified by Carollo et al. (2007). We find very little metallicity variation with pulsational phase for any of the stars. Combining their low metallicities with their large RVs, it is clear that our RRc sample is drawn from the Galactic halo population; none of the stars appear to be members of the thick disk.

Inspection of the relative abundance tables and figures suggests that the abundance ratios of our RRc sample are consistent with those of RHB, RRab, and BHB stars. The trends with [Fe/H] and $T_{\rm eff}$ appear to be essentially identical among all these HB groups. Second, it follows that since the RRc abundance ratios are in line with other HB stars, they are also consistent with other metal-poor evolutionary groups (red giant and main-sequence stars), as has been discussed in previous papers. In

Table 7
Average Abundances

Star[a]	$T_{\rm eff}$ [a]	log g[a]	v_t[a]	Fe I[b]	Fe II	Na I	Mg I	Al I	Si I	Si II	Ca I	Sc II	Ti II	Cr I	Cr II	Ni I	Sr II	Y II	Ba II
AS081933	7200	2.50	2.07	−2.89	−2.91	0.13	0.29	−0.49	0.25	1.17	0.37	0.26	0.43	−0.08	...	...	0.11	...	...
AS085254	7400	2.40	2.30	−1.53	−1.53	0.24	0.42	−0.70	0.31	0.04	0.26	0.07	0.26	−0.18	−0.02	...	0.57	−0.30	0.12
AS090900	7100	2.10	2.17	−1.79	−1.79	0.44	0.60	−0.50	−0.35	0.14	0.42	0.13	0.22	−0.14	−0.03	0.44	0.51	0.13	0.38
AS110522	7250	2.50	2.01	−1.79	−1.76	−0.14	0.40	−0.67	−0.28	0.39	0.43	0.17	0.33	−0.09	0.27	...	0.32	...	0.16
AS162158	7200	2.25	2.20	−1.84	−1.83	0.41	0.45	−0.40	0.00	0.52	0.18	0.07	0.24	−0.19	0.07	...	0.05	0.25	−0.15
AS200431	7100	2.17	1.76	−2.71	−2.73	0.01	0.50	−0.48	0.05	1.22	0.15	−0.04	0.34	0.01	0.23	...	−0.10	...	...
AS211933	7100	2.24	2.56	−1.52	−1.47	0.42	0.68	−0.72	−0.06	0.47	0.29	−0.02	0.32	−0.16	0.03	0.45	0.65	0.11	−0.13
AS230659	7100	2.04	2.15	−1.82	−1.84	0.59	0.63	−0.39	−0.23	0.53	0.31	−0.03	0.29	−0.19	0.09	...	1.02	0.35	0.17

Notes.
[a] Averaged over all phases.
[b] For Fe I and Fe II, the abundance units are [Fe/H]; for all other elements X, the abundance units are [X/Fe].

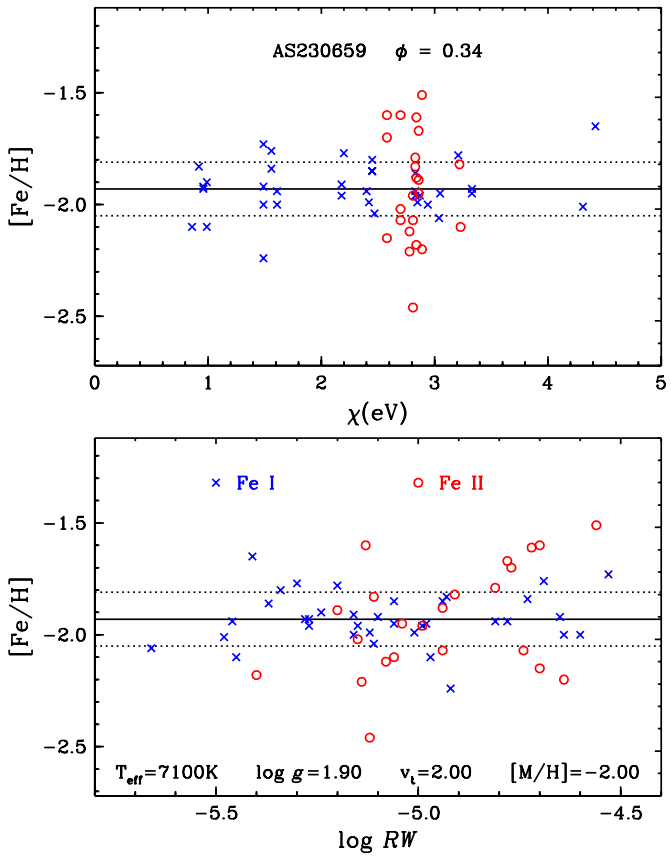

Figure 10. Abundances of individual Fe I and Fe II lines plotted as functions of excitation energy (χ, top panel) and reduced width (log RW, bottom panel) for star AS230659 at the co-added phase $\phi = 0.34$. The solid horizontal line represents the mean Fe abundance from Fe I at this phase, and the dotted lines represent the 1σ scatter value.
(A color version of this figure is available in the online journal.)

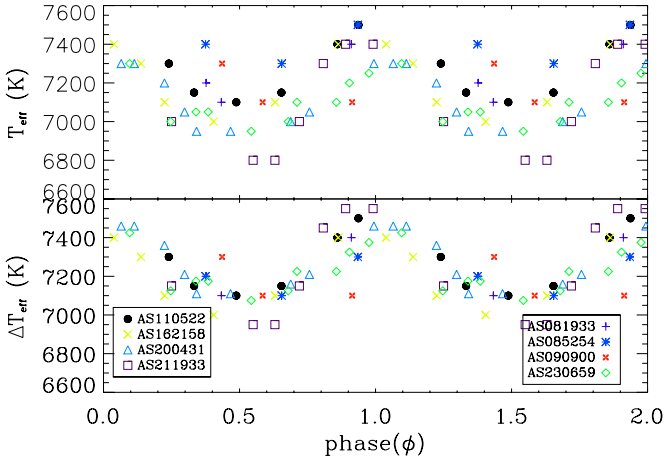

Figure 11. Effective temperatures as functions of pulsational phase for the program stars. In the top panel, the points are plotted as given in Table 4. In the bottom panel, the points for star AS110522 are plotted without change from the top panel; however for the seven other stars we have shifted their points by single offsets to match their mean $T_{\rm eff}$ values to that of AS110522. The resulting $T_{\rm eff}$–ϕ are labeled $\Delta T_{\rm eff}$, and they make clear the orderly temperature variations throughout the pulsational cycles that are common to RRc stars.
(A color version of this figure is available in the online journal.)

particular, all of the α and α-like elements (Mg, Si, Ca, and Ti) are enhanced ([X/Fe] $\simeq +0.3-+0.5$) just as they are in other metal-poor stars.

A few species deserve special comment. Non-LTE correction factors have been proposed for Na I, Al I, Si I, and Si II; see the discussion and references in For et al. (2011b). The strengths of Al I resonance lines are known to be affected by departures from LTE. Baumuller et al. (1997) computed corrections to LTE abundances for a variety of atmospheric parameters. However, the HB stars considered here have metallicities and $T_{\rm eff}$'s that encompass very large ranges: $-3 \lesssim$ [Fe/H] $\lesssim -1$ and

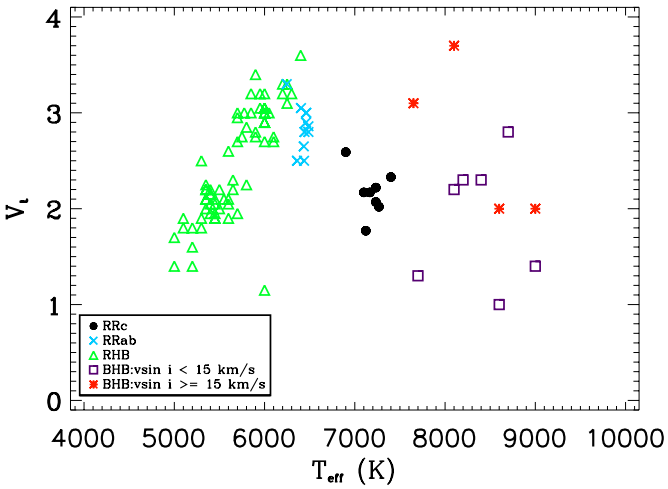

Figure 12. Microturbulent velocities of HB stars plotted as functions of their effective temperatures. The symbols are defined in the figure legend. Data for the RHB and BHB stars are taken from For & Sneden (2010), but the data for BHB stars are divided into slowly vs. rapidly rotating stars, as discussed in the text. The data for RRab stars (For et al. 2011b) and RRc stars (this study) are mean values over the pulsation cycles.
(A color version of this figure is available in the online journal.)

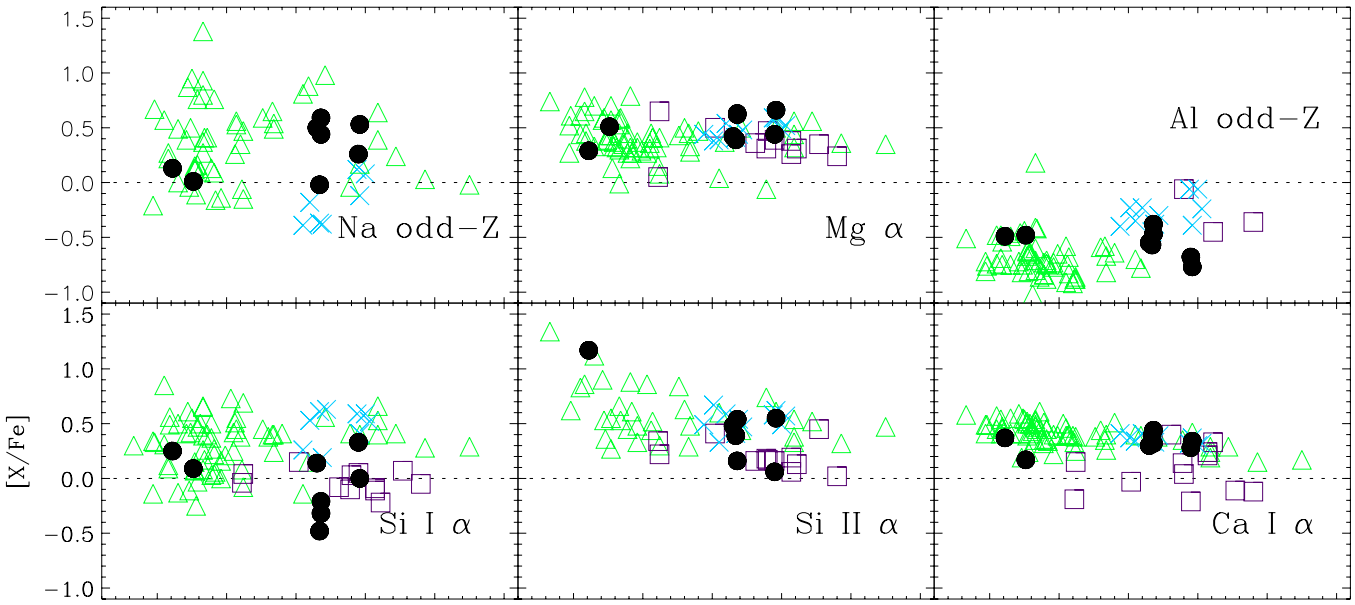

Figure 13. Relative abundance ratios for lighter elements as functions of [Fe/H] metallicity in the RRc program stars and other HB stellar samples. In all panels, the black filled circles are the RRc stars of this study, the green open triangles are for RHB stars (For & Sneden 2010), the blue ×'s are for RRab stars (For et al. 2011b), and the purple open squares are for BHB stars (For & Sneden 2010). The horizontal dotted lines in each panel represent the solar relative abundance ratio of that element, [X/Fe] = 0.

(A color version of this figure is available in the online journal.)

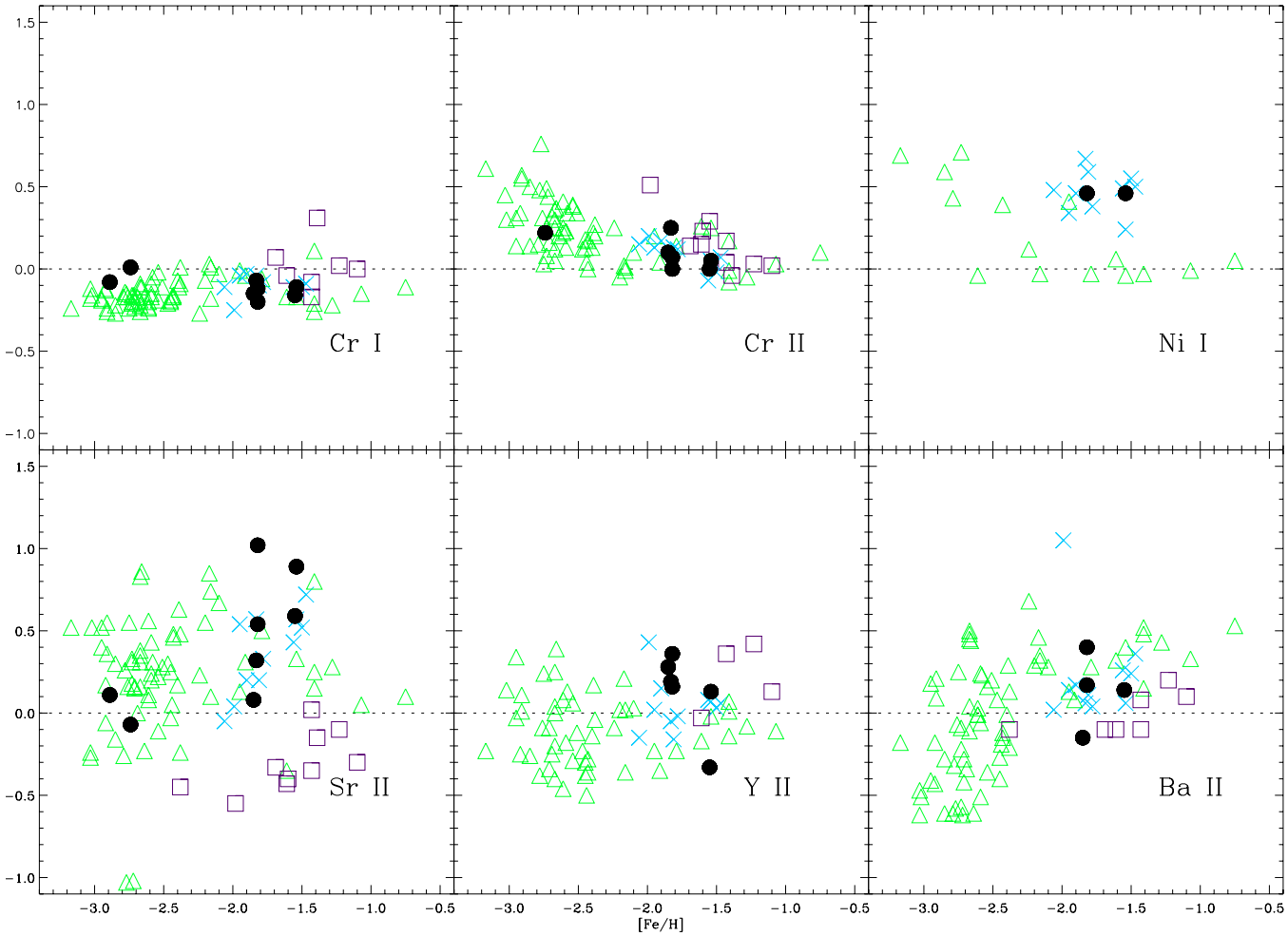

Figure 14. Relative abundance ratios for heavier elements as functions of [Fe/H] metallicity. The symbols and lines are as in Figure 13.

(A color version of this figure is available in the online journal.)

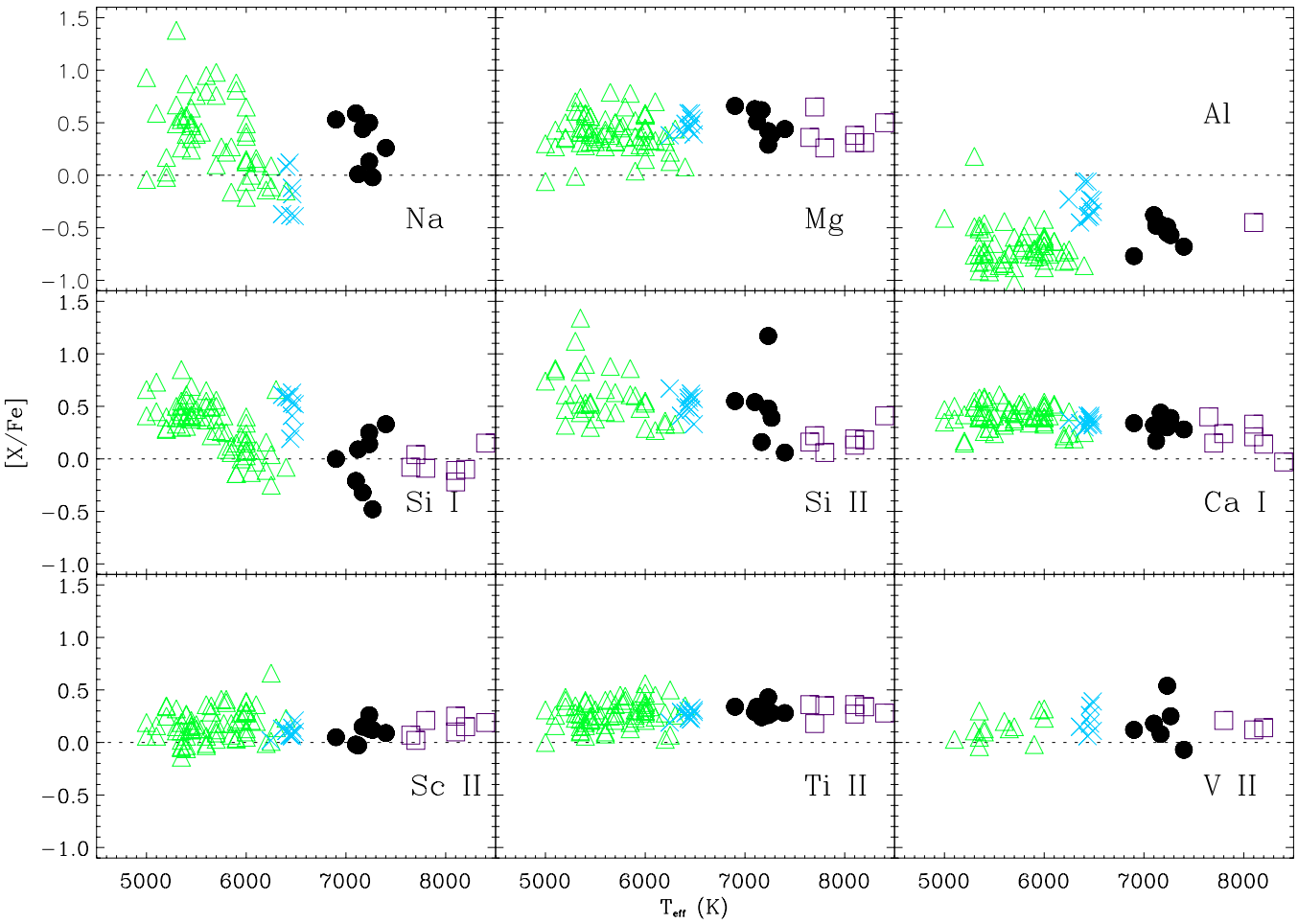

Figure 15. Relative abundance ratios for lighter elements as functions of $T_{\rm eff}$. The symbols and lines are as in Figure 13.
(A color version of this figure is available in the online journal.)

5000 K $\lesssim T_{\rm eff} \lesssim$ 9000 K. It is not at all clear that a one-size-fits-all non-LTE correction factor is physically realistic. Therefore we have chosen not to apply any non-LTE corrections to our RRc abundances. Furthermore, we have subtracted 0.65 dex from the RRab and BHB abundances to bring all Al abundances to a common scale for display in Figures 13 and 15. The acquired Al abundances appear to be consistent, which may signal that a single non-LTE correction is adequate to first approximation.

Metal-poor, giant stars generally seem to be relatively over-abundant in oxygen. EW measurements have been done for the oxygen triplet lines at 7771–7775 Å. On average, our [O/Fe] value is 1.74, which is unrealistically high. This value arrives from the fact that non-LTE effects are known to be large for these lines in HB stars (Clementini et al. 1995). Realistic statistical equilibrium calculations for the triplet in these pulsating stars would be difficult and beyond the scope of our work.

4.3. Metallicity Comparisons with Other Studies

For all but one of our program stars, no prior metallicity determinations have been reported in the literature. For AS211933 (YZ Cap) a few previous measurements of the Ca II K-line strength index (ΔS, Preston 1959) have been published. The ΔS parameter is defined from a comparison of an RRL star's hydrogen-line spectral type (ST(H)) and its Ca II K-line spectral type (ST(K)):

$$\Delta S = 10[\mathrm{ST(H)} - \mathrm{ST(K)}]. \quad (1)$$

These values are converted to metallicity estimates through calibrations using medium- and high-resolution spectroscopy (e.g., Butler 1975; Suntzeff et al. 1994; Gratton 1999; Clementini et al. 1995). All of these calibrations are of the form

$$[\mathrm{Fe/H}] = A\Delta S + B; \quad (2)$$

recommended values of the constants in this equation are similar in the various studies: $A = -0.17 \pm 0.02$ and $B = -0.2 \pm 0.2$.

Unfortunately, there is no general agreement on ΔS for AS211933. The original Preston (1959) study reported $\Delta S = 0.0$ on the basis of a single low-dispersion spectrogram. Subsequent measurements show a wide range: $\Delta S = 3.0$ (Butler 1975), 6.6 (Kemper 1982), 2.8 (Walker & Terndrup 1991), and 6.6 (Suntzeff et al. 1994). These values lead to metallicity estimates ranging from [Fe/H] ~ -0.2 to -1.3, if one uses the mean values of constants A and B. This metallicity range does not permit a meaningful comparison to our derived metallicity ([Fe/H] $= -1.54$ and -1.48 from lines of Fe I and Fe II, respectively).

Recently, Kollmeier et al. (2012) have completed a spectroscopic survey of 247 RRc variables selected from the ASAS database. The purpose of that study is to derive the mean absolute magnitude of this class of stars using the method of statistical parallax. Statistical parallaxes require space velocities, which in turn require RV values. Additionally, absolute magnitudes of RR Lyraes have a small dependence on their metallicities. Therefore Kollmeier et al. (2012) gathered high-resolution spectra for their target stars with the same telescope,

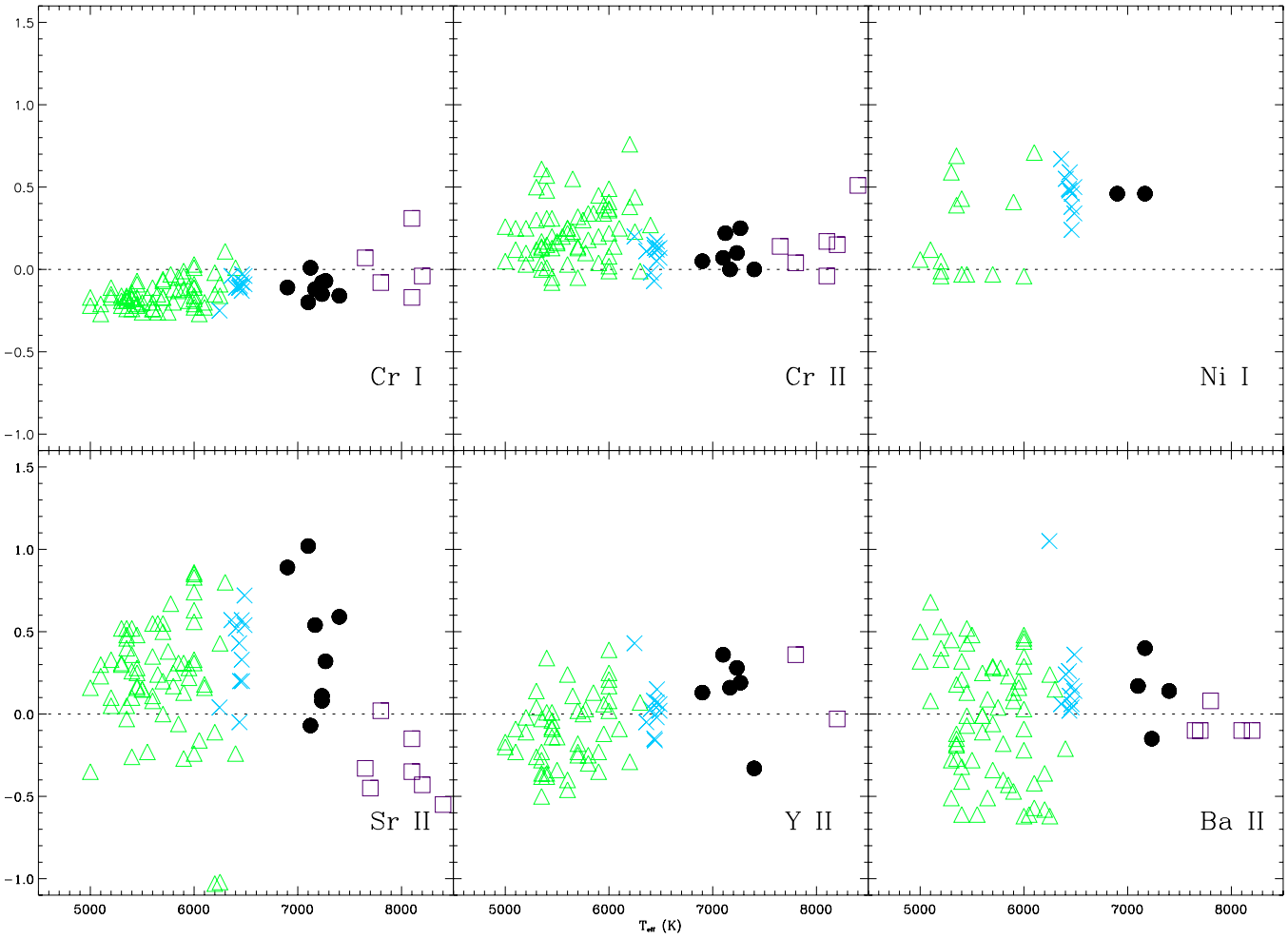

Figure 16. Relative abundance ratios for heavier elements as functions of $T_{\rm eff}$. The symbols and lines are as in Figure 13.
(A color version of this figure is available in the online journal.)

instrument, and observational setup as we have employed in our study.

For et al. (2011b) found that the optimal pulsational phase for atmospheric analyses of RRab stars is near $\phi \simeq 0.35$, in agreement with Kolenberg et al. (2010a). Near this phase, the star's photosphere is nearly at rest at its maximum expansion, the atmospheric micro- and macro-turbulence are smallest, the spectral lines are relatively sharp and symmetric, and atmospheric parameters $T_{\rm eff}$ and log g are not varying much. Additionally, the derived [Fe/H] metallicities proved to be relatively invariant over the RRab pulsational cycles. These properties carry over to the RRc variables, as demonstrated in the present work. Therefore in order to survey a large number of RRc variables, Kollmeier et al. (2012) opted to gather typically only 1−2 "snapshot" spectra per star, gathered in a pulsational phase interval of $\phi = 0.3-0.4$. Given the integration time limits for RRc's described in Section 2.2, their spectra are inevitably noisy: most have S/N = 15 ± 10.

Given these low S/N values and the intrinsically line-weak spectra of metal-poor RRc stars, Kollmeier et al. (2012) opted to compute grids of synthetic spectra with fixed $T_{\rm eff}$ and log g values in the wavelength ranges 4400−4680 Å and 5150−5450 Å and to estimate overall [Fe/H] metallicities from matching these syntheses to the observed spectra. No individual element abundance ratios were attempted with the snapshot spectra; see Section 3.3 of their paper for further details.

The RRc target selection for the Kollmeier et al. (2012) survey emphasized stars that do not have pronounced Blazhko light-curve modulations. Therefore we have only one star in common with their work: AS110522. From their snapshot spectrum, they estimate [Fe/H] $\simeq -1.80$, while we derived −1.83 from Fe I lines and −1.81 from Fe II lines, obviously in excellent agreement within observational and analytical errors.

To make a more meaningful comparison with Kollmeier et al. (2012), we processed individual spectra of our program stars through the metallicity pipeline of their study. The pulsational phase coverage of our spectra is not complete, and for stars AS090900 and AS211933 we have no observations in the phase range $\phi = 0.3$–0.4. However, since atmospheric parameters for our stars change only slowly, to increase the statistical sampling we used all the spectra for each star from $\phi = 0.25$–0.55 in this exercise. The number of spectra per star ranged from three to nine; the results are displayed in Figure 17. The error bars for our values represent the standard deviations, σ, of our [Fe/H] measurements per star from all of the co-added spectra, and the error bars for the grid synthesis values are the σ values from the various individual spectra of each star processed through the grid synthesis software. On average, $\langle [{\rm Fe/H}]_{\rm grid} - [{\rm Fe/H}]_{\rm GGPS} \rangle = -0.08 \pm 0.05$ ($\sigma = 0.13$), which we regard as a satisfactory agreement within the mutual uncertainties of the two methods of metallicity determination. Additionally, we find no obvious

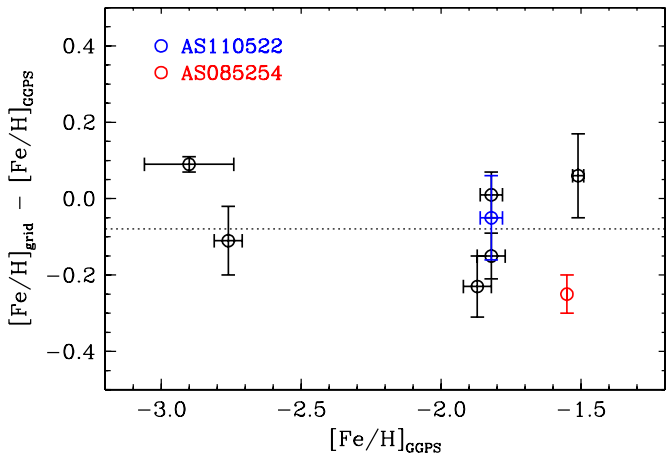

Figure 17. Comparison of our metallicities, $[Fe/H]_{GGPS}$, with those derived in the snapshot survey via grid syntheses by Kollmeier et al. (2012). The vertical axis is the difference in metallicities derived by their grid synthesis approach and those determined in this paper. The dotted line is the mean difference for these eight stars. The blue symbol for AS110522 denotes the one star in common between their study and ours. The red symbol for AS085254 calls attention to the largest discrepancy the metallicity estimates. See the text for further discussion.

(A color version of this figure is available in the online journal.)

trend with metallicity in this comparison in the interval $-1.5 \gtrsim [Fe/H] \gtrsim -2.9$ covered by our stars.

5. CONCLUSIONS

We have derived model atmospheric parameters, metallicities, and abundance ratios for eight field RRc variable stars. Each star has been observed 6−30 times, in most cases sampling nearly all of the pulsational phases. We used the echelle spectrograph of the Las Campanas du Pont Telescope to obtain all spectra for this study. The exposure times for our observations were necessarily short, and so we combined individual reduced spectra taken at similar phases into smaller sets in order to obtain higher S/N spectra for each star. Deriving $T_{\rm eff}$, log g, v_t, and [Fe/H] for all stars in all (co-added) phases yields metallicities that are essentially invariant with phase. Additionally, we find that the α-element (Mg, Si, Ca, Ti) abundances, on average, are overabundant ($[X/Fe] \simeq +0.3$ to 0.4) and the Fe-group elements (Sc, Cr, Ni) have solar abundance ratios ($[X/Fe] \simeq 0$) just as they are in other halo population samples. Finally, the [Fe/H] values of our program stars serve to calibrate the metallicity estimates of a large-sample RRc snapshot spectroscopic survey from Kollmeier et al. (2012).

This work has been supported by NSF grants AST-0908978 and AST-1211585 to C.S. and by the Baker Centennial Research Endowment to the Astronomy Department of the University of Texas. The John W. Cox Endowment for the Advanced Studies in Astronomy also supported this research project.

REFERENCES

Alonso, A., Arribas, S., & Martínez-Roger, C. 1999, A&AS, 140, 261
Balazs-Detre, J. 1964, ASPL, 9, 129
Baumuller, D. G., & Gehren, T. 1997, A&AS, 325, 1088
Behr, B. B. 2003a, ApJS, 149, 67
Behr, B. B. 2003b, ApJS, 149, 101
Blazhko, S. 1907, AN, 175, 327
Buchler, J. R., & Kolláth, Z. 2011, ApJ, 731, 24
Butler, D. 1975, ApJ, 200, 68
Butler, D., Carbon, D., & Kraft, R. P. 1976, ApJ, 210, 120
Butler, D., Kraft, R. P., & Kinman, T. D. 1979, AJ, 84, 993
Carollo, D., Beers, T. C., Lee, Y. S., et al. 2007, Natur, 450, 1020
Castelli, F., & Kurucz, R. L. 2003, in IAU Symp. 210, Modelling of Stellar Atmospheres, ed. N. Piskunov, W. W. Weiss, & D. F. Gray (Cambridge: Cambridge Univ. Press), 20
Chadid, M., Wade, G. A., Shorlin, S. L. S., & Landstreet, J. D. 2004, A&A, 413, 1087
Clementini, G., Carretta, E., Gratton, R., et al. 1995, AJ, 110, 2319
Cox, A. N. 2013, in Astrophys. Space Sci. Proc. 31, 77
For, B.-Q., Preston, G. W., & Sneden, C. 2011a, ApJS, 194, 38
For, B.-Q., & Sneden, C. 2010, AJ, 140, 1694
For, B.-Q., Sneden, C., & Preston, G. W. 2011b, ApJS, 197, 29
Gillet, D. 2013, A&A, 554, A46
Gratton, R. G. 1999, in Globular Clusters, ed. C. Martínez Roger, I. Perez Fournón, & F. Sánchez (Cambridge: Cambridge Univ. Press), 155
Helfer, H. L., Wallerstein, G., & Greenstein, J. L. 1959, ApJ, 129, 700
Kemper, E. 1982, AJ, 87, 1395
Kolenberg, K., & Bagnulo, S. 2009, A&A, 498, 543
Kolenberg, K., Fossati, L., Shulyak, D., et al. 2010a, A&A, 519, A64
Kolenberg, K., Szabó, R., Kurtz, D. W., et al. 2010b, ApJL, 713, L198
Kollmeier, J., Szczygieł, D. M., Burns, C. R., et al. 2013, ApJ, 775, 57
Kurucz, R. L. 1992, in IAU Symp. 149, The Stellar Populations of Galaxies, ed. B. Barbuy & A. Renzini (Dordrecht: Reidel), 225
Lambert, D. L., Heath, J. E., Lemke, M., & Drake, J. 1996, ApJS, 103, 183
Peterson, R. C., Carney, B. W., & Latham, D. W. 1996, ApJL, 465, L47
Peterson, R. C., Tarbell, T. D., & Carney, B. W. 1983, ApJ, 265, 972
Pojmański, G. 2003, AcA, 53, 341
Preston, G. W. 1959, ApJ, 130, 507
Preston, G. W. 2011, AJ, 141, 6
Preston, G. W., Shectman, S. A., & Beers, T. C. 1991, ApJ, 375, 121
Preston, G. W., & Sneden, C. 2000, AJ, 120, 1014
Preston, G. W., Sneden, C., Thompson, I. B., Shectman, S. A., & Burley, G. S. 2006, AJ, 132, 85
Ramírez, I., & Meléndez, J. 2005, ApJ, 626, 465
Skrutskie, M. F., Cutri, R. M., Stiening, R., et al. 2006, AJ, 131, 1163
Sneden, C. 1973, ApJ, 184, 839
Suntzeff, N. B., Kraft, R. P., & Kinman, T. D. 1994, ApJS, 93, 271
Szczygieł, D. M., & Fabrycky, D. C. 2007, MNRAS, 377, 1263
Walker, A. R., & Terndrup, D. M. 1991, ApJ, 378, 119